components is required to maintain the stability of the dynactin complex.

To test whether changes in p24 expression levels are sufficient to induce the figure eight chromosome alignment, we treated cells with siRNAs and then measured the expression levels of dynactin components and observed alterations in chromosome alignment. When cells were treated with siRNA-p150 for 24 or 48 h, expression levels of p24, dynamitin, and $p150^{Glued}$ relative to control cells were ~25% or higher (Fig. 6*B*), but no mitotic abnormalities were observed (Fig. 2, *A* and *C*). Treatment with siRNA-p150 for 72 h reduced the expression levels of dynamitin and $p150^{Glued}$ to <10% and p24 to ~20%, and this treatment induced metaphase arrest/delay and a few cells with the figure eight chromosome alignment (Fig. 2*C*). In contrast, treatment of cells with siRNA-p24 for 24 or 48 h reduced the expression levels of p24 to less than 15%, while maintaining relatively high (>25%) levels of dynamitin and $p150^{Glued}$. In this case, more mitotic cells showed a figure eight chromosome alignment (Fig. 2*C*).

We also treated HeLa(tc) cells with a combination of both siRNA-p24 and siRNA-p150 (50 or 100 nM each) for 72 h. Although this procedure reduced both p24 and p150 expression levels to ~10% of those in control cells (Fig. 6*C*, *lanes 2* and *3*), the ratio of cells in the figure eight alignment (42–45%) was virtually the same as cells treated with siRNA-p24 alone (43%, Fig. 6*D*), in which p24 and p150 expression are reduced to ~10 and 25% of control cells, respectively (Fig. 6*C*, *lane 4*). Once again, cells treated with siRNA-p150 alone that expressed p24 at 25% and p150 at 10% of control cells (*lane 5*) showed only a small number (~10%) of mitotic cells with the figure eight configuration (Fig. 6*D*). These data demonstrate that among all components of the dynactin complex, manipulation of p24 expression levels is most likely to result in cells assuming the figure eight configuration.

Further evidence in support of this correlation was observed when treated cells were immunostained simultaneously for p24 and $p150^{Glued}$. p24 immunofluorescence at centrosomes of mitotic HeLa(tc) cells treated with siRNA-p24 was markedly less intense in cells with the figure eight chromosome alignment relative to metaphasic cells in the same microscopic field (Fig. 6*E*, *panel 3*). Intriguingly, p150 immunofluorescence at centrosomes in most (23/25) of these figure eight cells was as bright as the signal in metaphasic cells (Fig. 6*E*, *panel 5*). In contrast, in cells treated with siRNA-p150, both p24 and p150 immunofluorescence signals in figure eight cells were markedly reduced (Fig. 6*E*, *panels 4* and *6*) in all cells observed (25/25). These results suggest that failure of p24 to accumulate in mitotic centrosomes induces figure eight chromosome alignment.

DISCUSSION

In this report, we treated HeLa and U2OS cells with siRNAs specific for p24 or $p150^{Glued}$, two components of the projecting arm of the dynactin complex. Time-lapse observations reveal that treatment of siRNA-p24 induces severe metaphase delay. In >40% of metaphase cells struggling to enter anaphase, chromosomes aligned on the metaphase plate break away and assume a configuration resembling a figure eight. In time, all cells with the figure eight alignment die without completing mitosis. In contrast with p24, cells treated with siRNA-p150 demonstrate severe delays in metaphase, but most cells do not assume the figure eight alignment and ultimately progress to anaphase. Neither p24 nor $p150^{Glued}$ appears to be involved in the progression of anaphase and telophase.

Reductions in p24 or $p150^{Glued}$ protein levels induce metaphase arrest/delay (Fig. 4*C* and supplemental Movies 1–3). This is consistent with a previous report in which cells overexpress dynamitin, which down-regulates dynactin function, also undergo metaphase arrest/delay (8). Failure to remove spindle checkpoint proteins such as BubR1 from kinetochores (Fig. 5*A*) results in metaphase delay because checkpoint proteins inhibit cdc20, a specific activator of the anaphase-promoting complex/cyclosome (reviewed in Ref. 20). Because anaphase-promoting complex/cyclosome functions as an E3 ubiquitin ligase, mitotic checkpoint proteins that are remain on kinetochores delay ubiquitin-dependent degradation of cyclin B1 (Fig. 5*B*) or securin, which then inhibits cohesin hydrolysis and blocks chromosome segregation (Fig. 5*C*).

Nonetheless, the transition of chromosomes from a metaphase to a figure eight configuration does not appear to be a direct result of spindle checkpoint protein retention at kinetochores. Because there is a marked reduction of γ-tubulin and CG-NAP signals at mitotic centrosomes in cells with the figure eight chromosome alignment (Fig. 5*E*), insufficient amounts of γ-TuRC in metaphase centrosomes appear to be one of the major factors driving the phenotype. Thus, we hypothesize that loss of spindle microtubule tension (Fig. 5*D*) is the defect that induces chromosomes to break away from alignment at the metaphase plate.

The two functions of the dynactin complex are to remove spindle checkpoint proteins from kinetochores and to maintain centrosome integrity until entry into anaphase. Although we have observed that neither of these functions are disturbed when expression levels of p24, dynamitin, or $p150^{Glued}$ remain at least 25% of control levels (siRNA-p150 for 48 h, see Figs. 2*C* and 6*A*), we did note that a 10-fold reduction in the expression of either p24 or $p150^{Glued}$ impaired the removal of checkpoint proteins, resulting in metaphase delay. In contrast, chromosome integrity and the resulting formation of figure eight cells was only induced with a 10-fold reduction in p24 levels but not with a reduction in $p150^{Glued}$. Immunofluorescence experiments also emphasized a correlation between accumulation of p24 (but not $p150^{Glued}$) in centrosomes and figure eight chromosome alignment (Fig. 6*E*). These data suggest that p24 acts independently of $p150^{Glued}$ in metaphase centrosomes, where it helps maintain chromosome integrity and prevents breakaway until entry into anaphase.

Although it is generally accepted that p24, dynamitin, and $p150^{Glued}$ function together in the dynactin projecting arm (2), we and others (4, 21) have observed that the localization of different dynactin components during mitosis varies considerably. For example, p24 immunofluorescence is strong at centrosomes relative to mitotic spindles or kinetochores. This is particularly evident during early anaphase (Fig. 1, *E* and *F*)

when p150^{Glued} immunofluorescence is barely detectable. In conclusion, our results suggest that p24 operates independently from the dynactin complex in binding to metaphase centrosomes and maintaining their integrity. To explore this hypothesis further, we are currently investigating the function of p24 in metaphase centrosomes in greater detail.

Acknowledgments—We thank Dr. K. Kevin Pfister (University of Virginia) for kindly providing antibodies against p24, Dr. M. Katsuno and G. Sobue (Nagoya University) for providing expression vectors for p150^{Glued}, and M. Nakamura for excellent technical assistance.

REFERENCES

1. Musacchio, A., and Salmon, E. D. (2007) *Nat. Rev. Mol. Cell Biol.* **8,** 379–393
2. Schroer, T. A. (2004) *Annu. Rev. Cell Dev. Biol.* **20,** 759–779
3. Pfister, K. K., Benashski, S. E., Dillman, J. F., 3rd, Patel-King, R. S., and King, S. M. (1998) *Cell Motil Cytoskeleton* **41,** 154–167
4. Karki, S., LaMonte, B., and Holzbaur, E. L. (1998) *J. Cell Biol.* **142,** 1023–1034
5. Eckley, D. M., and Schroer, T. A. (2003) *Mol. Biol. Cell* **14,** 2645–2654
6. Amaro, I. A., Costanzo, M., Boone, C., and Huffaker, T. C. (2008) *Genetics* **178,** 703–709
7. Burkhardt, J. K., Echeverri, C. J., Nilsson, T., and Vallee, R. B. (1997) *J. Cell Biol.* **139,** 469–484
8. Whyte, J., Bader, J. R., Tauhata, S. B., Raycroft, M., Hornick, J., Pfister, K. K., Lane, W. S., Chan, G. K., Hinchcliffe, E. H., Vaughan, P. S., and Vaughan, K. T. (2008) *J. Cell Biol.* **183,** 819–834
9. Cheung, P. Y., Zhang, Y., Long, J., Lin, S., Zhang, M., Jiang, Y., and Wu, Z. (2004) *J. Biol. Chem.* **279,** 45308–45311
10. Dixit, R., Levy, J. R., Tokito, M., Ligon, L. A., and Holzbaur, E. L. (2008) *J. Biol. Chem.* **283,** 33611–33619
11. Oshimori, N., Ohsugi, M., and Yamamoto, T. (2006) *Nat. Cell Biol.* **8,** 1095–1101
12. Katsuno, M., Adachi, H., Minamiyama, M., Waza, M., Tokui, K., Banno, H., Suzuki, K., Onoda, Y., Tanaka, F., Doyu, M., and Sobue, G. (2006) *J. Neurosci.* **26,** 12106–12117
13. Soneoka, Y., Cannon, P. M., Ramsdale, E. E., Griffiths, J. C., Romano, G., Kingsman, S. M., and Kingsman, A. J. (1995) *Nucleic Acids Res.* **23,** 628–633
14. Burns, J. C., Friedmann, T., Driever, W., Burrascano, M., and Yee, J. K. (1993) *Proc. Natl. Acad. Sci. U.S.A.* **90,** 8033–8037
15. Kuribara, R., Kinoshita, T., Miyajima, A., Shinjyo, T., Yoshihara, T., Inukai, T., Ozawa, K., Look, A. T., and Inaba, T. (1999) *Mol. Cell. Biol.* **19,** 2754–2762
16. Kuribara, R., Honda, H., Matsui, H., Shinjyo, T., Inukai, T., Sugita, K., Nakazawa, S., Hirai, H., Ozawa, K., and Inaba, T. (2004) *Mol. Cell. Biol.* **24,** 6172–6183
17. Tokai-Nishizumi, N., Ohsugi, M., Suzuki, E., and Yamamoto, T. (2005) *Mol. Biol. Cell* **16,** 5455–5463
18. Shinjyo, T., Kuribara, R., Inukai, T., Hosoi, H., Kinoshita, T., Miyajima, A., Houghton, P. J., Look, A. T., Ozawa, K., and Inaba, T. (2001) *Mol. Cell. Biol.* **21,** 854–864
19. Shi, Q., and King, R. W. (2005) *Nature* **437,** 1038–1042
20. Lu, Y., Wang, Z., Ge, L., Chen, N., and Liu, H. (2009) *Cell Struct. Funct.* **34,** 31–45
21. Echeverri, C. J., Paschal, B. M., Vaughan, K. T., and Vallee, R. B. (1996) *J. Cell Biol.* **132,** 617–633

The *Samd9L* Gene: Transcriptional Regulation and Tissue-Specific Expression in Mouse Development

Qiujie Jiang[1], Benjamin Quaynor[1], Alex Sun[1], Qiaoli Li[1], Hirotaka Matsui[2], Hiroaki Honda[3], Toshiya Inaba[2], Eli Sprecher[4] and Jouni Uitto[1]

Normophosphatemic familial tumoral calcinosis (NFTC) is caused by mutations in the *SAMD9* gene. This gene is absent in mouse, while there is a murine paralog, *Samd9*-like (*Samd9L*). To clarify the relationships between *SAMD9* and *SAMD9L*, we investigated the transcriptional regulation and expression pattern of mouse *Samd9L*. An ~1.5-kb mouse *Samd9L* promoter fragment was cloned, and a series of 5′ deletion constructs were linked to a luciferase reporter gene. All constructs showed significant activity in transfected epithelial cells and mouse fibroblasts, and the presence of regulatory *cis*-elements as close as 87 bp upstream of the transcription start site was identified. Ras-responsive element binding protein 1 (Rreb-1) was identified in this region by protein–DNA binding array. The expression of *Samd9L* was upregulated by calcitonin, and this was preceded by a significant increase in the expression of *Rreb-1* mRNA. Quantitative real-time PCR analysis of *Samd9L* revealed near-ubiquitous expression, with the highest level in the kidney. Tissue-specific expression was also confirmed both by *in situ* β-gal staining and quantitative enzymatic activity assay in a transgenic *Samd9L*$^{+/-}$ mouse in which the *LacZ* gene replaced exon 2 in the *Samd9L* gene. These findings assist in understanding the regulation of *Samd9L* in the context of its paralogous gene, *SAMD9*, which harbors mutations in NFTC.

Journal of Investigative Dermatology advance online publication, 17 March 2011; doi:10.1038/jid.2011.61

INTRODUCTION

Familial tumoral calcinosis (MIM610455) is a group of heritable disorders characterized by ectopic mineralization of the extracellular matrix of connective tissues (Sprecher, 2010). The normophosphatemic variant, NFTC, manifests with extensive mineralization of cutaneous tissues, associated with inflammatory manifestations mostly evident in mucosal tissues. Recently, mutations in NFTC have been demonstrated in sterile alpha motif domain-containing 9 gene (*SAMD9*), which encodes a cytoplasmic protein with currently unknown function (Topaz *et al.*, 2006; Chefetz *et al.*, 2008). The *SAMD9* gene is located in the human chromosome 7q21 region, and next to it in head-to-tail orientation is a paralogous gene, *SAMD9*-like (*SAMD9L*), both with similar structures in that there is one large, ~5–6 kb coding exon that is preceded upstream by a large intron and either one (*SAMD9L*) or several (*SAMD9*) relatively small non-coding exons (Li *et al.*, 2007). Both human genes encode a putative protein of ~170–190 kb with 58% sequence homology, which in their amino-terminal segments display a well-conserved sterile alpha motif domain potentially involved in protein/protein interactions.

In a recent study, gene expression differences were noted between cell cultures derived from an aggressive fibromatosis tumor as compared with control tissue (Li *et al.*, 2007). In particular, reduced *SAMD9* expression was noted in aggressive fibromatosis, as well as in 20% of cases of breast cancer and 35% of cases of colon cancer cell lines compared with normal tissues. Thus, SAMD9 may have a role in regulating cell proliferation and suppressing the neoplastic phenotype. Recently, a common microdeletion cluster in the 7q21.3 subband region has been identified in patients with myeloid leukemia and myelodysplastic syndrome (Asou *et al.*, 2009). This microdeletion region contains three genes, *SAMD9*, *SAMD9L*, and *Miki*, which were postulated as candidates for myeloid tumor suppressor genes on 7q. Finally, SAMD9 has been suggested to be a key molecule controlling cancer cell death in malignant glioma by Sendai virus particle or interferon-β treatment (Tanaka *et al.*, 2010). With respect to ectopic mineralization, it was noted that the NFTC patients generally develop calcium deposits in areas subject to repeated trauma and associated with marked inflammatory manifestations, suggesting that *SAMD9* may also have a role in the inflammatory response to tissue injury. It has been speculated that TNF-α, a proinflammatory

[1]*Department of Dermatology and Cutaneous Biology, Jefferson Medical College, Philadelphia, Pennsylvania, USA;* [2]*Department of Molecular Oncology, Research Institute for Radiation Biology & Medicine, Hiroshima University, Hiroshima, Japan;* [3]*Department of Developmental Biology, Research Institute for Radiation Biology & Medicine, Hiroshima University, Hiroshima, Japan and* [4]*Department of Dermatology, Tel Aviv Sourasky Medical Center, Tel Aviv, Israel*

Correspondence: Jouni Uitto, Department of Dermatology and Cutaneous Biology, Jefferson Medical College, 233 S. 10th Street, Suite 450 BLSB, Philadelphia, PA 19107, USA. E-mail: Jouni.Uitto@jefferson.edu

Abbreviations: NFTC, normophosphatemic familial tumoral calcinosis; Rreb-1, Ras-responsive element binding protein 1; Samd9L, sterile alpha motif domain-containing 9-like

Received 17 November 2010; revised 14 January 2011; accepted 27 January 2011

cytokine that links inflammation and apotosis, might have a role in *SAMD9* regulation (Sprecher, 2010). Besides these observations, the physiological roles of *SAMD9* and *SAMD9L* are poorly understood.

An intriguing observation is that while an orthologous gene of human *SAMD9* exists in rat, the corresponding gene is lost in mouse lineage owing to a unique genomic rearrangement (Li *et al.*, 2007). However, mice do have the ortholog to human *SAMD9L*, but very little is known of the regulation of the *Samd9/Samd9L* gene–gene system either in human or in mouse. In this study, we have specifically explored the spatial and temporal expression of the *Samd9L* gene during mouse development, as well as in a novel mouse "knockout" model in which part of the *Samd9L* coding region has been replaced by the *LacZ* gene.

RESULTS AND DISCUSSION

To gain insight into the tissue-specific expression of *Samd9L*, a multiple mouse tissue panel was first screened for the corresponding mRNA by quantitative real-time (RT)-PCR. The results indicated high level of expression in kidney, followed by spleen, stomach, and adrenal gland, when the level of expression was normalized for mouse actin mRNA in the same samples (Figure 1a). This near-ubiquitous expression of mouse *Samd9L* is consistent with previous findings by Li *et al* (2007) and Topaz *et al* (2006), who demonstrated that *SAMD9* and *SAMD9L* are expressed in all human adult, fetal, and tumor tissues that were available from human multiple tissue complementary DNA (cDNA) panels. During mouse embryonic development at days 8.5 and 9.5, essentially no expression was detected (Figure 1a, lanes 17 and 18), but low levels were detectable at days 12.5 and 19 (Figure 1a, lanes 19 and 20). RT-PCR of mouse kidney revealed low, yet detectable levels of *Samd9L* mRNA at birth, and the expression levels significantly increased during the subsequent 2 and 4 weeks of life (Figure 1b and c). Computerized scanning analysis indicated that no further change in the *Samd9L* mRNA levels in mouse kidney was noted between 4 and 40 weeks of life (Figure 1c).

To examine the transcriptional control of *Samd9L* gene expression, an expression construct extending from −1,428 to +98 was developed, and a number of 5′-deletion constructs were generated and linked to firefly luciferase reporter (Figure 2a). Transfection of four cell lines, including three epithelial cells and a mouse fibroblast cell line (NIH3T3), in culture with these reporter plasmids showed significant level of expression over controls mock transfected with the basic vector (Figure 2b). The activity in epithelial

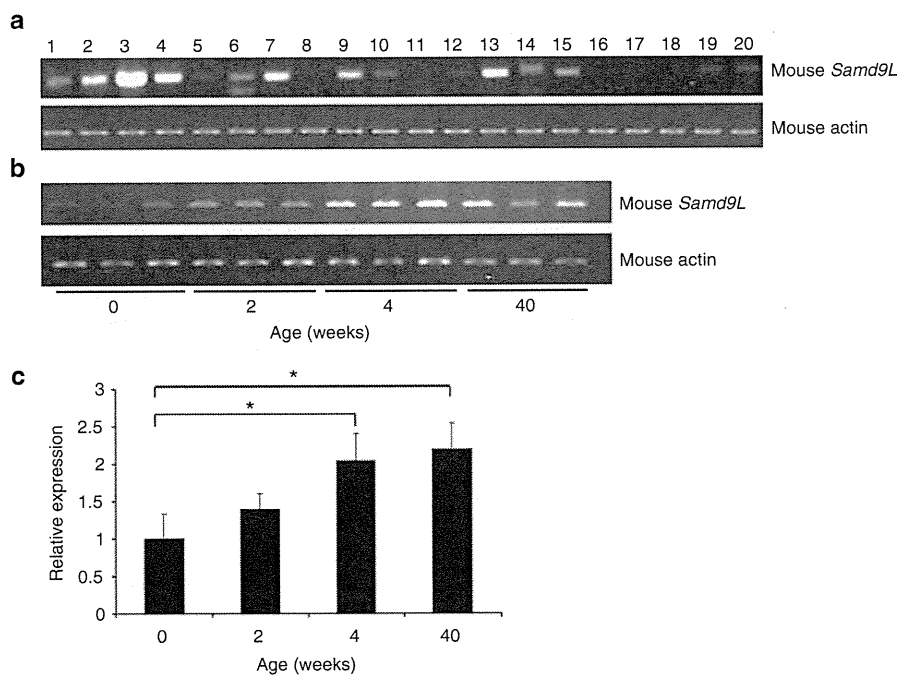

Figure 1. *Samd9L* expression is tissue-specific and developmentally regulated. (**a**) *Samd9L* messenger RNA (mRNA) expression was assessed by PCR using a pre-standardized complementary DNA library of multiple mouse tissues. The represented tissues are as follows: 1. Brain; 2. Heart; 3. Kidney; 4. Spleen; 5. Thymus; 6. Liver; 7. Stomach; 8. Small intestine; 9. Muscle; 10. Lung; 11. Testis; 12. Skin; 13. Adrenal gland; 14. Pancreas; 15. Uterus; 16. Prostate gland; 17. Embryo/day 8.5; 18. Embryo/day 9.5; 19. Embryo/day 12.5; 20. Embryo/day 19. (**b**) The kidneys were harvested from the mice at the different ages. Real-time (RT)-PCR analysis revealed that the expression of mouse *Samd9L* in the kidneys increased with age when mice at the age of 0 (newborn), 2, 4, and 40 weeks were examined. (**c**) The levels of *Samd9L* mRNA expression were quantified by determining the pixel intensities of the bands of RT-PCR products on the images in (**b**) using a computer program (ImageQuant, Molecular Dynamics, Sunnyvale, CA), and normalized with those of the corresponding internal actin controls. Data from three independent measurements were used (mean ± SD). The relative expression of mouse *Samd9L* was calculated using the mRNA level of mouse *Samd9L* in the newborns as 1 (*$P<0.05$).

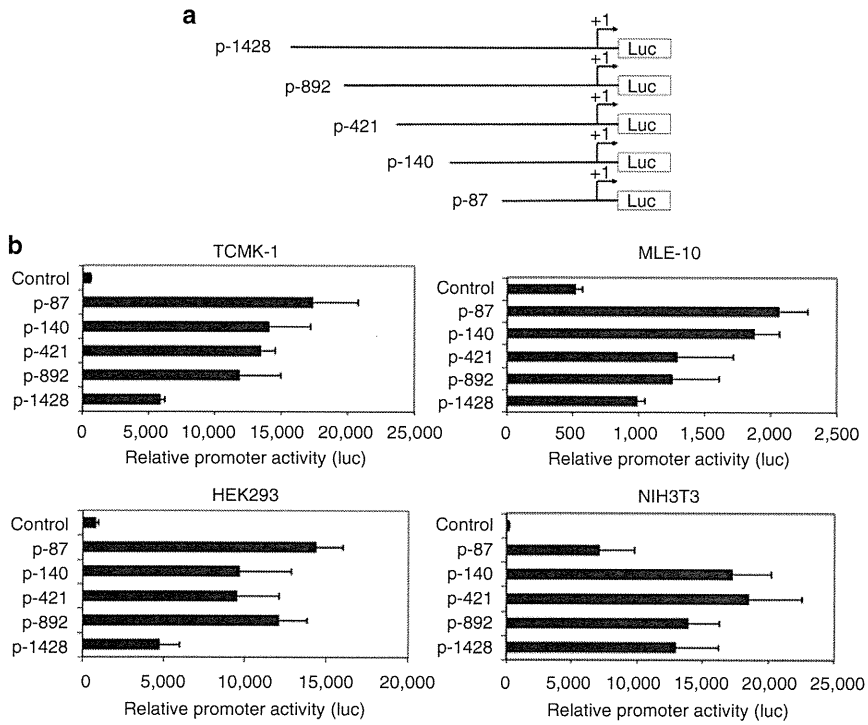

Figure 2. Serially truncated 5′ deletion constructs of the mouse *Samd9L* promoter display significant activities in various cell lines. (**a**) Serial deletion constructs of the mouse *Samd9L* 5′-flanking region were inserted upstream of firefly luciferase gene (Luc) in the reporter plasmid pGL3-Basic. The numbers on the left indicate the 5′-position of the construct, starting from the transcription start site (+1; arrow). (**b**) The *Samd9L* promoter constructs (0.75 μg) described in (**a**) or the control pGL3-Basic vector were cotransfected with 0.25 μg of pRSV-β-galactosidase reporter plasmid into the indicated cell types using FuGENE6 reagent (Roche). The cells were lysed 50 hours later and assayed for luciferase and β-galactosidase activities. Luciferase activity was divided by β-galactosidase activity to correct for transfection efficiency. The data are presented as the mean ± SD of three separate experiments, each performed in triplicate. HEK293, human embryonic kidney epithelial cell line; MLE-10, mouse liver epithelial cell line; NIH3T3, mouse skin fibroblast cell line; TCMK-1, mouse kidney epithelial cell line.

cell cultures (TCMK-1, MLE-10, and human embryonic kidney (HEK293) revealed that the shortest construct tested, p-87-luciferase, showed the highest level of expression. Inclusion of upstream sequences up to −1,428 resulted in reduction of the activity, suggesting the presence of down-regulatory elements. In all cultures, co-transfection of a β-galactosidase expression plasmid (pRSV-β-gal) was included, followed by β-galactosidase enzyme activity determination, which was used to correct for transfection efficiencies. The mouse fibroblast cell line (NIH3T3) showed reduced activity by about 50% with the p-87 construct as compared with other constructs tested containing the upstream sequences (Figure 2b, lower right panel). It appears, therefore, that the proximal promoter region within the segment −87 to +98 contains the essential sequences necessary for high level of expression particularly in epithelial cell cultures.

By searching for transcription factors that might regulate the expression of the *Samd9L* promoter within the p-87 promoter fragment, nuclear extracts of NIH3T3 cells were tested in a protein/DNA filter array containing 96 transcription factors. A number of transcription factors were identified to bind to the target sequence in p-87; however, search for consensus sequences within the p-87 fragment identified the corresponding cognate binding sites for only two of them, E47 and Ras-responsive element binding protein (Rreb; Figures 3a and b). E47 is widely expressed and binds specifically to the immunoglobulin κ-chain enhancer κE2. It shows homology to other proteins with a Helix–Loop–Helix dimerization domain signature of the MYC type. E47 has been reported to be essential for normal B-cell hematopoiesis (Frasca *et al.*, 2003). RREB is a zinc-finger transcription factor that binds to RAS-responsive elements of gene promoters (Zhang *et al.*, 2003). It has been shown that the calcitonin gene promoter contains an RAS-responsive element and that RREB-1 binds to it and increases expression of calcitonin (Mukhopadhyay *et al.*, 2007; Flajollet *et al.*, 2009).

As RREB has been suggested to be responsive to calcitonin, we tested the possibility that *Samd9L* gene expression might be mediated by calcitonin through Rreb, one of the transcription factors shown to bind to the proximal −87 promoter sequence. Incubation of NIH3T3 cells with calcitonin showed over threefold increase in *Samd9L* gene expression, which was statistically significant at 4 and 7 days of incubation (Figure 4a). Parallel assay of Rreb mRNA levels by RT-PCR revealed a statistical increase as early as at the 24-h point (Figure 4b).

To demonstrate the specificity of Rreb binding to the promoter activity, transient cell transfections were done with

a

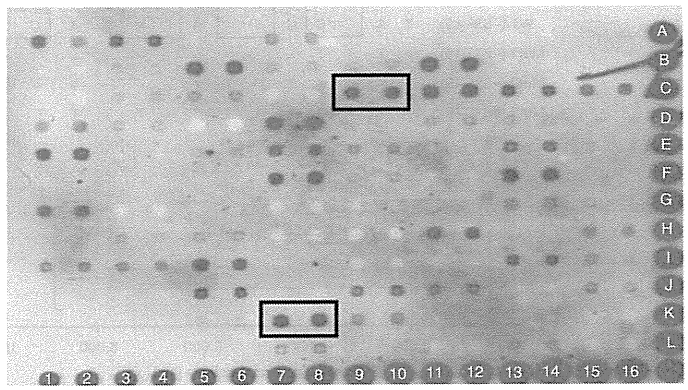

c

-87-AGGTCTTTGGGTTTTACCCAAACAAACCAGCAGGTGGCATAGTTGGCACTAAA
RREB
SRY
E47
+1
GAGCAGAAAAAGAGAAAAAAAGCATTTCAGGAAGTCTCTTTCTGTATCAGAA
HNF-3b
c-Ets-
TCGAAACTGGAAACTGAAGCAGAGGTGGTTTTTTACTTCCTTACACTCTTGCCA
GCATTAGCCACACC -+98

b

ADR1	ADR1	AhR/ Arnt	AhR/ Arnt	ANG-IRE	ANG-IRE	Antiox. RE	Antiox. RE	AP3	AP3	AP4 (RIP60)	AP4 (RIP60)	β-resp. element	β-resp. element	CdxA/ NKX2	CdxA/ NKX2	A
CEF1	CEF1	CEF2	CEF2	CETF/ CRE	CETF/ CRE	COUP-TF	COUP-TF	CREB-BP1	CREB-BP1	c-Rel	c-Rel	DR-0	DR-0	DR-1	DR-1	B
DR-2	DR-2	DR-3	DR-3	DR-4	DR-4	DR-5	DR-5	E47	E47	E4BP4	E4BP4	E4F,ATF	E4F,ATF	EIK1	EIK1	C
EVI-1	EVI-1	FKHR (human)	FKHR (human)	Fkhr (mouse)	Fkhr (mouse)	Afxh (Foxo4)	Afxh (Foxo4)	Freac-2 (1)	Freac-2 (1)	Freac-2 (2)	Freac-2 (2)	Freac-4	Freac-4	DR-0 Freac-7	Freac-7	D
GAG	GAG	GAS	GAS	GATA-1	GATA-1	GATA-1/2	GATA-1/2	GATA-2	GATA-2	GATA-3	GATA-3	GATA-4	GATA-4	GATA-6	GATA-6	E
Gfi-1	Gfi-1	HAS	HAS	HBS	HBS	HBS + HAS	HBS + HAS	HFH-1	HFH-1	HFH-2	HFH-2	HFH-3	HFH-3	HFH-8	HFH-8	F
HIF-1	HIF-1	HNF-3	HNF-3	HNF-3β	HNF-3β	HNF-4	HNF-4	HNF-4/COUP-TF	HNF-4/COUP-TF	IkaroS	IkaroS	IRF-1/2	IRF-1/2	ISRE(1)	ISRE(1)	G
ISRE(2)	ISRE(2)	ISRE (transTF)	ISRE (transTF)	L-III BP	L-III BP	KKLF	KKLF	MEF-2(1)	MEF-2(1)	MEF-2(2)	MEF-2(2)	MEF-3	MEF-3	MSP1	MSP1	H
MT-box	MT-box	MUSF1	MUSF1	MZF1	MZF1	NF-Y	NF-Y	Nkx-2.5	Nkx-2.5	NPAS2	NPAS2	HBS/ xbp-1	HBS/ xbp-1	NZF-3	NZF-3	I
ORE	ORE	p300	p300	PARP	PARP	Pax2	Pax2	Pax3	Pax3	Pax4	Pax4	Pax6	Pax6	Pax8	Pax8	J
PPARa	PPARa	PPARr	PPARr	RREB(1)	RREB(1)	RREB (2)	RREB (2)	RSRFC4	RSRFC4	SAA	SAA	Skn	Skn	SRY	SRY	K
Tax/ CREB	Tax/ CREB	TCF/LEF	TCF/LEF	XBP-1	XBP-1	XRE	XRE	ZIA	ZIA	ZIB	ZIB	ZIC	ZIC	ZID	ZID	L
1	2	3	4	5	6	7	8	9	10	11	12	13	14	15	16	

Figure 3. Protein/DNA array identifies select transcription factors binding to the mouse *Samd9L* promoter region. (**a**) Hybridization signals of the transcription factors bound to the p-87 promoter fragment identified in nuclear extracts of NIH3T3 cells. The TranSignal protein/DNA filter contains 96 transcription factors, each tested in duplicate (adjacent horizontal dots). (**b**) The transcription factors identified by the protein/DNA array as binding to *Samd9L* promoter region are indicated on shaded background. The selected transcription factors whose putative recognition sites were identified by TFSEARCH (version 1.3, Kyoto University, Japan) in the p-87 promoter fragment are outlined by black frame in (**a**) and (**b**). Insufficient signal was noted for those factors shown on the white background. (**c**) The sequence extending from −87 to +98 was scanned for transcription factor-binding sites by using TFSEARCH. The putative recognition sites for select transcription factors identified in DNA are indicated below the sequence. The transcription initiation site is referred to by +1.

the wild-type p-87 plasmid reporter construct together with three mutant constructs in which segments of the consensus binding site of Rreb (-63/-49) were mutated (Figure 5a). The wild-type construct showed over fourfold level of expression of the luciferase reporter gene as compared with the control plasmid (Figure 5b). No change was noted with Mutant 1, while Mutant 2 showed approximately threefold increase over the wild-type activity. Mutant 3 essentially abolished the promoter activity (Figure 5b). Interestingly, the Mutant 2 also mutates the consensus binding site of SRY, a testis-determining factor, which has been reported to also have a role in hormonal influence on calcification (Yamada *et al.*, 2006). Further studies, such as those investigating gender differences in *SAMD9L* expression, are needed to understand the role of androgens in these processes.

The tissue-specific expression of the *Samd9L* promoter was also assessed in *in vivo* situations by examination of a heterozygous transgenic mouse in which exon 2 of the gene was replaced by *LacZ* gene (*Samd9L*$^{+/-}$), and therefore the expression of β-galactosidase was under the *Samd9L* upstream regulatory sequences within the promoter. It should be noted that these *Samd9L*$^{+/-}$ mice, as well as their homozygous counterparts, develop acute myelogenous leukemia at high frequency after they reach the age of 20 months. This mouse model has been preliminarily reported (Matsui *et al.*, 2009), and a detailed manuscript is in preparation (Matsui et al., unpublished). Dissection of different tissues in *Samd9L*$^{+/-}$ mice followed by β-galactosidase staining confirmed the highest levels of expression in the kidney and spleen, while the level of expession was very low in the liver and the muscle (Figure 6a). Histochemical staining of paraffin-embedded sections for β-galactosidase revealed expression in both proximal and distal tubules (Figure 6c). The localization of Samd9L protein in mouse kidney was further confirmed by immunohistochemical staining of paraffin sections of wild-type mouse kidney with

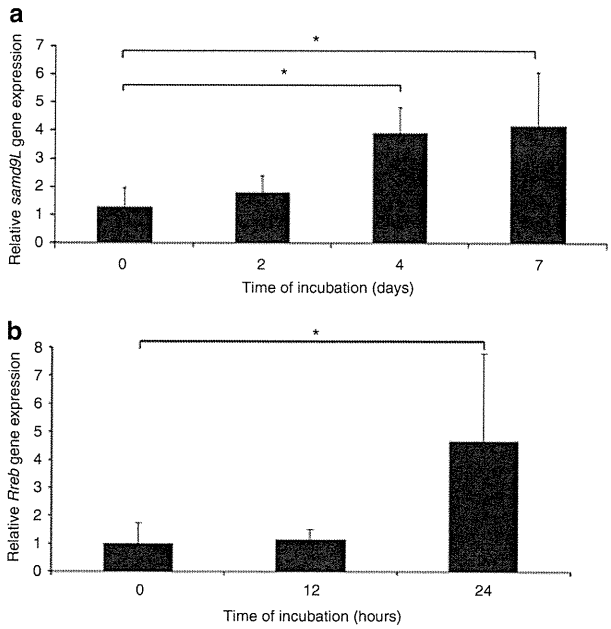

Figure 4. Calcitonin enhances the expression of mouse *Samd9L* and *Rreb* genes in NIH3T3 cells *in vitro*. Real-time (RT)-PCR was performed using total RNA isolated from NIH3T3 cells cultured with 200 ng/l calcitonin for the indicated time periods using primers specific for *Samd9L*, *Rreb*, and *Gapdh*, as described in Materials and Methods. The data were normalized to the *Gapdh* endogenous control and are presented as fold change relative to untreated cells (0 time point). *Samd9L* expression is presented in the top panel (**a**) and *Rreb* expression in the bottom panel (**b**). Asterisks indicate statistical significance ($P<0.05$) when compared with the corresponding controls.

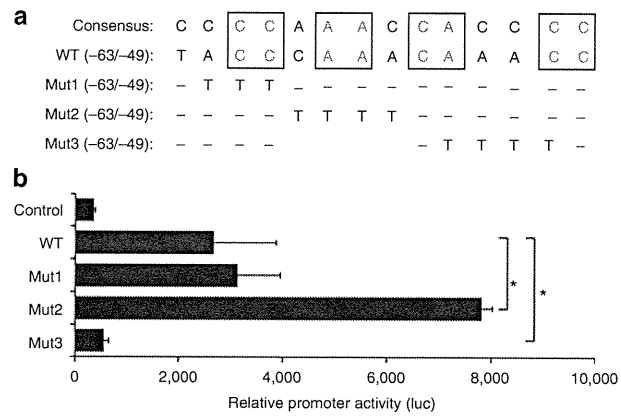

Figure 5. Mutations in the Rreb binding site sequences alter the activity of *Samd9L* gene promoter. (**a**) Sequences for the published (Thiagalingam *et al.*, 1996) consensus sequence for the RREB binding site and wild-type (WT) sense strand of the p-87 plasmid construct (sequence homology boxed), as well as mutated plasmids (Mut 1, Mut 2, Mut 3) developed by site-directed mutagenesis with mutant primers, as described in Materials and Methods, are indicated in the figure. (**b**) The WT and mutant constructs were cotransfected with pRSV-β-galactosidase plasmid (0.75 and 0.25 μg, respectively) into NIH 3T3 cells using FuGENE6 (Roche), lysed after 50 hours of incubation, and then assayed for luciferase activity (Luc), which was normalized by β-galactosidase activity to correct for transfection efficiency. The data are presented as the mean ± SD of three independent experiments each performed in triplicate. Asterisks indicate statistical significance ($P<0.05$) when compared with the WT construct.

a Samd9L primary antibody, which revealed expression in tubules, but not in the glomeruli (Figure 6d).

The expression of β-galactosidase was also quantitatively measured by enzymatic activity assay in the extracts from the same tissues that were stained for β-gal *in situ* (Figure 6b). Highest level of enzymatic activity, as determined spectrophotometrically at 570 nm, after deduction of the background reflecting endogenous β-galactosidase activity, showed that the highest levels were observed in the kidney and the spleen, confirming the results obtained by RT-PCR at the level of mRNA expression, as shown in Figure 1a, and by β-galactosidase staining *in situ* (Figure 6a).

In summary, the present study of mouse *Samd9L* revealed near-ubiquitous expression, with the highest level in the kidney, a major organ regulating calcium-phosphate homeostasis and the site of calcitonin hormonal action. The transcriptional regulation of *Samd9L* as explored in this study adds to our understanding of the potential role of this gene in carcinogenesis. This information, in the context of the regulation of the *SAMD9* gene expression, may contribute to our understanding of mineralization processes, such as those taking place in NFTC.

MATERIALS AND METHODS

Animals

The *Samd9L* "knockout" mouse model was developed by homologous recombination resulting in replacement of exon 2 in the *Samd9L* gene by the *LacZ* gene (Matsui *et al.*, 2009). C57/BL6 mice were obtained from Jackson Labs (Bar Harbor, ME). All animal studies were performed in accordance with the institutional guidelines of Thomas Jefferson University Animal Care and Use Committee and the National Institutes of Health. Mice were placed in cages in a temperature-controlled room with a 12-hour light–dark cycle and free access to food and water.

Cell culture

All cell lines (NIH3T3, mouse skin fibroblasts; HEK293, human embryonic kidney epithelial cells; MLE-10, mouse liver epithelial cells; and TCMK-1, mouse kidney epithelial cells) were cultured in Dulbecco's modified Eagle's medium and supplemented with 10% heat-inactivated fetal bovine serum, 2 mM; L-glutamine, 100 IU ml^{-1} penicillin, and 100 μg ml^{-1} streptomycin (Cellgro, Mediatech, Herndon, VA). Cultures were maintained at 37°C in a humidified atmosphere of 5% CO_2 and 95% air.

Antibodies

Antibodies to mouse *Samd9L* were raised in rabbits to the peptide WPENKELDEDSTLIEC (Abgent, San Diego, CA). 4′-6-Diamidino-2-phenylindole was purchased from Invitrogen (Eugene, OR).

Immunofluorescence

Whole-mouse kidney was embedded in paraffin and cut into 8-μm sections onto slides. The slides were then deparaffinized, permeabilized, and stained with anti-mouse Samd9L antibody at 1:500 dilution followed by Texas Red secondary (red) antibody at 1:300 dilution and counterstained with 4′-6-diamidino-2-phenylindole (blue) at 1:5000 dilution, or only stained with Texas Red secondary

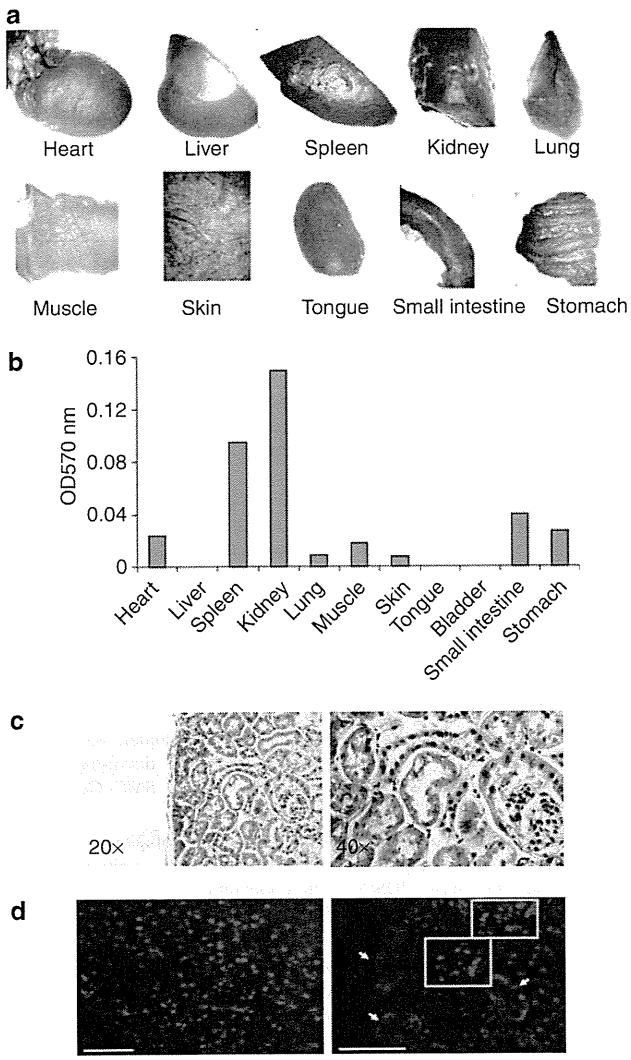

Figure 6. Assessment of *Samd9L* reveals tissue-specific expression *in vivo*. (**a**) Various organs were harvested from *Samd9L*$^{+/-}$ mice, in which the *LacZ* gene replaced exon 2 in the *Samd9L* gene in one allele, and were analyzed by *in situ* β-galactosidase (β-gal) staining. (**b**) Tissue-specific expression was analyzed by quantitative enzymatic activity assay in a transgenic *Samd9L*$^{+/-}$ mouse. The β-gal activity in each tissue of the wild-type (WT) mice was used as the baseline, and the data were expressed after normalization to the corresponding baselines and to the protein content of each extract. The highest β-gal enzymatic activity was observed in the kidney and spleen. (**c**) Paraffin sections of the β-gal-stained kidney confirmed localization in both proximal and distal tubules. (**d**) Paraffin sections of WT mouse kidney were stained with Samd9L primary antibody and Texas Red secondary antibody and counterstained with 4′-6-diamidino-2-phenylindole (DAPI) (right panel), or stained only with Texas Red secondary antibody and DAPI (left panel). The Samd9L was expressed in the tubules (arrows) but not in the glomeruli (in rectangles). Scale bar, 100 μm.

antibody at 1:300 dilution and counterstained with 4′-6-diamidino-2-phenylindole to serve as a control.

Promoter plasmid constructs

The serially truncated *Samd9L* promoter fragments, with their 5′-ends ranging from −1428 to −87 and their 3′-end being fixed at +98, were prepared by PCR amplification of mouse genomic DNA using sense primers containing a *Mlu*I restriction site, and all of the constructs shared the same antisense primer containing an *Nhe*I restriction site (Supplementary Table S1 online). The PCR products were separated by gel electrophoresis and extracted from a gel slice (Qiagen, Valencia, CA), then cloned into pCR-Blunt II-TOPO vector using ZeroBlunt TOPO PCR Cloning kit (Invitrogen, Carlsbad, CA). The plasmid was then digested with *Mlu*I and *Nhe*I and cloned into pGL3-Basic luciferase vector (Promega, Madison, WI). Mutagenesis of the Rreb-binding site in the p-87 reporter construct, spanning from −87 to +98, was performed by site-directed mutagenesis using the QuikChange XL Site-Directed Mutagenesis kit (Stratagene, La Jolla, CA) and the manufacturer's instructions with specific primers. The final constructs were sequenced in both directions to ensure correct nucleotide sequence. Computer analysis of the promoter region of *Samd9L* was conducted to detect putative *cis*-acting elements using a transcription factor database (TFSEARCH, Kyoto University, version 1.3).

Transient transfections and luciferase assay

Plasmid constructs used for transient transfection were prepared using a purification kit (Qiagen). All cell lines (NIH3T3, HEK293, MLE-10, TCMK-1) were plated on a 24-well plate 24 hours prior to transfection and grown to approximately 80% confluency. The cells in each well were cotransfected with 0.75 μg of experimental plasmid and 0.25 μg of pRSV-β-galactosidase expression plasmid as an internal control for transfection efficiency, using FuGENE6 transfection reagent according to the manufacturer's instructions (Roche Diagnostic, Indianapolis, IN). After incubation for 50 hours, the transfected cells were harvested and assayed as previously described. Each experiment was performed in triplicate.

Quantitative expression of mRNA in mouse tissues

RapidScan gene expression cDNA arrays containing mouse tissues for quantitative PCR were purchased from OriGene (Rockville, MD). These arrays contained prestandardized amounts of cDNA from 20 independent mouse tissues. The cDNA was amplified by PCR using primers specific for *Samd9L* (sense, located in exon 1: 5′-CCTGGTGTCTC TCAGCCAGT-3′; antisense, located in exon 2: 5′-CTTCATTCTGCCCT GTCTCC-3′). PCR products were separated by gel electrophoresis on a 2% agarose gel and stained with ethidium bromide.

RNA extraction and reverse transcription-PCR

NIH3T3 cells were plated on 100-mm dishes 24 hours prior to treatment and allowed to grow to 60% confluence. The cells were then washed with PBS and incubated with media containing 200 ng/l calcitonin (American Peptide Company, Sunnyvale, CA) for the indicated time period. Total RNA was extracted from NIH3T3 cells using an RNeasy Mini Kit (Qiagen) following the manufacturer's instructions. Total RNA was treated with DNase I to eliminate amplification of genomic DNA. The amount and quality of RNA were verified by measuring the absorbance at 260/280 nm. Random-primed reverse transcription of RNA was performed with the Superscript First-Strand Synthesis System for RT-PCR (Invitrogen).

SYBR Green PCR amplification was performed in a model 7000 sequence detector (Applied Biosystems, Foster City, CA). The reactions were carried out in a 96-well plate in a 25 μl reaction volume containing 12.5 μl of 2 × SYBR Green PCR Master Mix

(Applied Biosystems), 0.3 nM concentrations of forward and reverse primers each, and 10 ng of cDNA. Initial incubation at 95°C for 15 min was followed by 40 cycles of 95 °C for 15 seconds and either 56 °C (for *Samd9L*) or 60 °C (for *Rreb*) for 1 minute. NIH3T3 cDNA samples in triplicate were used in each run. The amount of specific mRNA in each RNA sample was quantified and normalized to *Gapdh* mRNA. The relative expression level of the target genes was calculated using the ΔΔCt method (Real-time PCR software; model 7000 sequence detector; Applied Biosystems). Reaction specificity was determined by the dissociation curve immediately after the last reaction cycle, and visualized with the software Dissociation Curve 1.0 (7000 sequence detection system; Applied Biosystems).

Protein/DNA array

A 187-bp fragment of the *Samd9L* promoter region, extending from −87 to +98, was excised from the p-87 construct with restriction enzymes *Mlu*I and *Nhe*I, and labeled with biotin using Bio-16-dUTP (Roche, Mannheim, Germany) and the Klenow fragment of DNA polymerase I (Invitrogen). Unincorporated Bio-16-dUTP was removed by a spin column and the biotin-labeled DNA fragment was coupled to M-280 streptavidin magnetic beads (Dynal Biotech, Oslo, Norway) using the manufacturer's conditions. The DNA-coupled magnetic beads were incubated with 500 μg protein from NIH3T3 nuclear extract for 2 hours at 4°C in the binding buffer as previously described. After washing, the bound proteins were dissociated from the DNA-coupled beads by incubating in a buffer containing 2 M NaCl for 60 minutes on ice. The bound proteins extracted from the 187-bp promoter region fragment were incubated with the TranSignal (Panomics, Redwood, CA) probe mix, a set of 96 biotin-labeled DNA oligonucleotides corresponding to the consensus sequences for the corresponding transcription factors, to allow the formation of DNA/protein complexes. The transcription-factor bound probes were isolated and then dissociated from the DNA/protein complex and used to hybridize the TranSignal Array spotted with complementary consensus-binding sequences of the transcription factor probes according to the manufacturer's instructions. Hybridization signals were visible after exposure to X-ray film following chemiluminescent detection.

β-Gal staining and quantitative enzymatic activity assay

To analyze the biodistribution and expression of the mouse Samd9L, various tissues were isolated from adult *Samd9L*$^{+/-}$ mice and examined for beta-galactosidase expression *in vivo*. The tissues fixed with 4% paraformaldehyde were stained for β-galactosidase using a LacZ Detection kit (InvivoGen, San Diego, CA). The sections were lightly counterstained with neutral red before mounting. For the enzyme activity assays, the various tissues were harvested from either *Samd9L*$^{+/-}$ mice or wild-type mice, and tissue extracts were analyzed for beta-galactosidase using a β-gal assay kit (Invitrogen) (Payet *et al.*, 1998). The beta-galactosidase activity in each tissue from wild-type mice was used as the baseline. The data were expressed after normalization to the corresponding baselines and to the protein content in each extract.

Statistical analysis

Statistical differences between the means in various groups were calculated by Student's two-tailed *t*-test.

CONFLICT OF INTEREST

The authors state no conflict of interest.

ACKNOWLEDGMENTS

We thank Alix Grand-Pierre and Carol Kelly for assistance. This study was supported by the DHHS, through NIH/NIAMS grants R01 AR28450 (JU) and K08 AR057099 (QJ). Qiaoli Li is the recipient of a Dermatology Foundation Research Career Development Award.

SUPPLEMENTARY MATERIAL

Supplementary material is linked to the online version of the paper at http://www.nature.com/jid

REFERENCES

Asou H, Matsui H, Ozaki Y *et al.* (2009) Identification of a common microdeletion cluster in 7q21.3 subband among patients with myeloid leukemia and myelodysplastic syndrome. *Biochem Biophys Res Commun* 383:245–51

Chefetz I, Ben Amitai D, Browning S *et al.* (2008) Normophosphatemic familial tumoral calcinosis is caused by deleterious mutations in SAMD9, encoding a TNF-alpha responsive protein. *J Invest Dermatol* 128:1423–9

Flajollet S, Poras I, Carosella ED *et al.* (2009) RREB-1 is a transcriptional repressor of HLA-G. *J Immunol* 183:6948–59

Frasca D, Nguyen D, Riley RL *et al.* (2003) Decreased E12 and/or E47 transcription factor activity in the bone marrow as well as in the spleen of aged mice. *J Immunol* 170:719–26

Li CF, MacDonald JR, Wei RW *et al.* (2007) Human sterile alpha motif domain 9, a novel gene identified as down-regulated in aggressive fibromatosis, is absent in the mouse. *BMC Genomics* 8: 92–109

Matsui H, Nagamachi A, Ozaki Y *et al.* (2009) Loss of *Titan* (*Samd9L*), a candidate -7/9q- responsible gene encoding an actin remodeling regulator, develops MDS/AML in cooperation with *Evi1* or *Fbx/10*. *ASH Annual Meeting and Exposition*, New Orleans, LA, USA, abstract 2963

Mukhopadhyay NK, Cinar B, Mukhopadhyay L *et al.* (2007) The zinc finger protein ras-responsive element binding protein-1 is a coregulator of the androgen receptor: implications for the role of the Ras pathway in enhancing androgenic signaling in prostate cancer. *Mol Endocrinol* 21:2056–70

Payet V, Arnauld C, Picault JP *et al.* (1998) Transcriptional organization of the avian adenovirus CELO. *J Virol* 72:9278–85

Sprecher E (2010) Familial tumoral calcinosis: from characterization of a rare phenotype to the pathogenesis of ectopic calcification. *J Invest Dermatol* 130:652–60

Tanaka M, Shimbo T, Kikuchi Y *et al.* (2010) Sterile alpha motif containing domain 9 is involved in death signaling of malignant glioma treated with inactivated Sendai virus particle (HVJ-E) or type I interferon. *Int J Cancer* 126:1982–91

Thiagalingam A, De Bustros A, Borges M *et al.* (1996) RREB-1, a novel zinc finger protein, is involved in the differentiation response to Ras in human medullary thyroid carcinomas. *Mol Cell Biol* 16: 5335–45

Topaz O, Indelman M, Chefetz I *et al.* (2006) A deleterious mutation in SAMD9 causes normophosphatemic familial tumoral calcinosis. *Am J Hum Genet* 79:759–65

Yamada T, Hirotaka K, Koshizuka Y *et al.* (2006) Carminerin contributes to chondrocyte calcification during endochondral ossification. *Nat Med* 12:665–70

Zhang S, Xiaolan Q, Chanelle R *et al.* (2003) $p16^{INK4a}$ gene promoter variation and differential binding of a repressor, the ras-responsive zinc-finger transcription factor, RREB. *Oncogene* 22:2285–95

Rapid Emergence of Telaprevir Resistant Hepatitis C Virus Strain from Wildtype Clone *In Vivo*

Nobuhiko Hiraga,[1,2] Michio Imamura,[1,2] Hiromi Abe,[1,2] C. Nelson Hayes,[1,2] Tomohiko Kono,[1,2] Mayu Onishi,[1,2] Masataka Tsuge,[1,2] Shoichi Takahashi,[1,2] Hidenori Ochi,[2,3] Eiji Iwao,[4] Naohiro Kamiya,[4] Ichimaro Yamada,[4] Chise Tateno,[2,5] Katsutoshi Yoshizato,[2,5] Hirotaka Matsui,[6] Akinori Kanai,[7] Toshiya Inaba,[6] Shinji Tanaka,[1,2] and Kazuaki Chayama[1,2,3]

Telaprevir is a potent inhibitor of hepatitis C virus (HCV) NS3-4A protease. However, the emergence of drug-resistant strains during therapy is a serious problem, and the susceptibility of resistant strains to interferon (IFN), as well as the details of the emergence of mutant strains *in vivo*, is not known. We previously established an infectious model of HCV using human hepatocyte chimeric mice. Using this system we investigated the biological properties and mode of emergence of mutants by ultra-deep sequencing technology. Chimeric mice were injected with serum samples obtained from a patient who had developed viral breakthrough during telaprevir monotherapy with strong selection for resistance mutations (A156F [92.6%]). Mice infected with the resistant strain (A156F [99.9%]) developed only low-level viremia and the virus was successfully eliminated with interferon therapy. As observed in patients, telaprevir monotherapy in viremic mice resulted in breakthrough, with selection for mutations that confer resistance to telaprevir (e.g., a high frequency of V36A [52.2%]). Mice were injected intrahepatically with HCV genotype 1b clone KT-9 with or without an introduced resistance mutation, A156S, in the NS3 region, and treated with telaprevir. Mice infected with the A156S strain developed lower-level viremia compared to the wildtype strain but showed strong resistance to telaprevir treatment. Although mice injected with wildtype HCV showed a rapid decline in viremia at the beginning of therapy, a high frequency (11%) of telaprevir-resistant NS3 V36A variants emerged 2 weeks after the start of treatment. *Conclusion:* Using deep sequencing technology and a genetically engineered HCV infection system, we showed that the rapid emergence of telaprevir-resistant HCV was induced by mutation from the wildtype strain of HCV *in vivo*. (HEPATOLOGY 2011;54:781-788)

Chronic hepatitis C virus (HCV) infection is a leading cause of cirrhosis, liver failure, and hepatocellular carcinoma.[1,2] The current standard treatment for patients chronically infected with HCV is the combination of peg-interferon (PEG-IFN) and ribavirin (RBV).[3-5] However, this treatment results in sustained viral response (SVR), defined as negative for HCV RNA 24 weeks after cessation of the therapy, in only about 50% of patients with genotype 1 HCV infection with high viral loads.[3-5] Given the low

Abbreviations: HCV, hepatitis C virus; HSA, human serum albumin; PEG-IFN, peg-interferon; RBV, ribavirin; RT-PCR, reverse transcript-polymerase chain reaction; SCID, severe combined immunodeficiency; SVR, sustained viral response; uPA, urokinase-type plasminogen activator.

From the [1]Department of Medicine and Molecular Science, Division of Frontier Medical Science, Programs for Biomedical Research, Graduate School of Biomedical Sciences, Hiroshima University, Hiroshima, Japan; [2]Liver Research Project Center, Hiroshima University, Hiroshima, Japan; [3]Laboratory for Digestive Diseases, RIKEN Center for Genomic Medicine, Hiroshima, Japan; [4]Research and Development Unit, Mitsubishi Tanabe Pharma Corp., Yokohama, Japan; [5]PhoenixBio Co., Ltd., Higashihiroshima, Japan; [6]Department of Molecular Oncology and Leukemia Program Project, Research Institute for Radiation Biology and Medicine, Hiroshima University, Hiroshima, Japan; [7]Radiation Research Center for Frontier Science, Research Institute for Radiation Biology and Medicine, Hiroshima University, Hiroshima, Japan.

Received January 17, 2011; accepted May 16, 2011.

Supported in part by a grant-in-aid for Scientific Research from the Japanese Ministry of Labor, Health and Welfare

Address reprint requests to: Prof. Kazuaki Chayama, M.D., Ph.D., Department of Medical and Molecular Science, Division of Frontier Medical Science, Programs for Biomedical Research, Graduate School of Biomedical Science, Hiroshima University, 1-2-3 Kasumi, Minami-ku, Hiroshima 734-8551, Japan. E-mail: chayama@hiroshima-u.ac.jp; fax: +81-82-255-6220.

View this article online at wileyonlinelibrary.com.

DOI 10.1002/hep.24460

Potential conflict of interest: E.I., N.K., I.Y. are employees of Mitsubishi Tanabe Pharma Corp. The other authors have nothing to declare.

effectiveness of the current therapy, many molecules have been screened for antiviral activity against HCV for use in development of novel anti-HCV therapies. A number of new selective inhibitors of HCV proteins, the so-called STAT-C (specifically targeted antiviral therapy for HCV) inhibitors, are currently under development. Telaprevir is a reversible, selective, specific inhibitor of the HCV NS3-4A protease that has shown potent antiviral activity in HCV replicon assays.[6] Although the antiviral effect of telaprevir is quite potent, monotherapy using these drugs results in rapid emergence of drug-resistant strains.[7,8] Accordingly, these drugs are used in combination with pegylated-IFN and ribavirin for chronic hepatitis C patients. Because the HCV virus replicates rapidly and RNA polymerase lacks a proofreading system, HCV viral quasispecies can emerge *de novo*, and some of these variants may confer resistance. Although a resistant variant is initially present at low frequency, it may quickly emerge as the dominant species during antiviral treatment.[9,10] Resistant clones against HCV NS3-4A protease inhibitors have reportedly been induced in replicon systems.

The immunodeficient urokinase-type plasminogen activator (uPA) mouse permits repopulation of the liver with human hepatocytes, resulting in human hepatocyte chimeric mice that are able to develop HCV viremia after injection of serum samples positive for the virus.[11] We and other groups have reported that the human hepatocyte chimeric mouse is useful for evaluating the effect of NS3-4A protease inhibitor.[12,13] Using this mouse model, we developed a reverse genetics systems for HCV.[14,15] This system is useful to study characteristics of HCV strains with various substitutions of interest because the confounding effects of quasispecies can be minimized. Using ultra-deep sequencing technology, we demonstrate the rapid emergence of telaprevir resistance in HCV as a result of mutation from wildtype strain using genetically engineered HCV-infected human hepatocyte chimeric mice.

Materials and Methods

Animal Treatment. Generation of the $uPA^{+/+}$/$SCID^{+/+}$ mice and transplantation of human hepatocytes were performed as described recently by our group.[16] All mice were transplanted with frozen human hepatocytes obtained from the same donor. Mice received humane care and all animal protocols were performed in accordance with the guidelines of the local committee for animal experiments. Infection, extraction of serum samples, and sacrifice were performed under ether anesthesia. Mice were injected either intravenously with HCV-positive human serum samples or intrahepatically with *in vitro*-transcribed genotype 1b HCV RNA. HCV-infected mice were administered either perorally with 200-300 mg/kg of telaprevir (VX950; MP424; Mitsubishi Tanabe Pharma, Osaka, Japan) twice a day or intramuscularly with 1,500 IU/g of IFN-alpha (Dainippon Sumitomo Pharma, Tokyo). The telaprevir dose was determined in a previous study in which this dosage range was found to yield serum concentrations equivalent to treated human patients.[13]

Human Serum Samples. After obtaining written informed consent, human serum samples containing genotype 1b HCV were obtained from two patients with chronic hepatitis. The individual serum samples were divided into aliquots and stored separately in liquid nitrogen until use. The study protocol conforms to the ethical guidelines of the 1975 Declaration of Helsinki and was approved *a priori* by the Institutional Review Committee.

HCV RNA Transcription and Inoculation into Chimeric Mice. We have previously established an infectious genotype 1b HCV clone HCV-KT9 derived from a Japanese patient with severe acute hepatitis (GenBank access. no. AB435162).[15] We cloned this HCV complementary DNA (cDNA) into plasmid pBR322 under a T7 RNA promoter to create the plasmid pHCV-KT9. Ten μg of plasmid DNA, linearized by *Xba*I (Promega, Madison, WI) digestion, were transcribed in a 100 μL reaction volume with T7 RNA polymerase (Promega) at 37°C for 2 hours and analyzed by agarose gel electrophoresis. Each transcription mixture was diluted with 400 μL of phosphate-buffered saline (PBS) and injected into the livers of chimeric mice.[15] The QuikChange site-directed mutagenesis kit (Stratagene, Foster City, CA) was used to introduce a substitution at amino acid 156 of the NS3 region (A156S).

RNA Extraction and Amplification. RNA was extracted from serum samples by Sepa Gene RV-R (Sankojunyaku, Tokyo), dissolved in 8.8 μL RNase-free H_2O, and reverse transcribed using a random primer (Takara Bio, Shiga, Japan) and M-MLV reverse transcriptase (ReverTra Ace, Toyobo, Osaka, Japan) in a 20-μL reaction mixture according to the instructions provided by the manufacturer. Nested polymerase chain reaction (PCR) and quantitation of HCV by Light Cycler (Roche Diagnostic, Japan, Tokyo) were performed as reported.[15]

Ultra-Deep Sequencing. We adapted multiplex sequencing-by-synthesis to simultaneously sequence

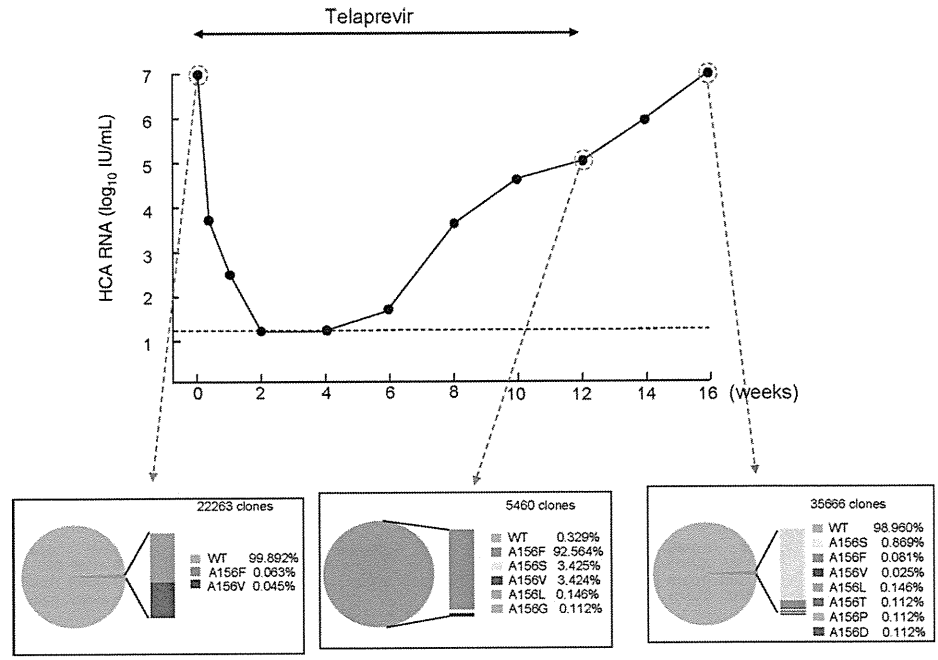

Fig. 1. Changes in serum HCV RNA levels in a telaprevir-treated chronic hepatitis C patient. A 55-year-old woman infected with genotype 1b HCV was treated with 750 mg of telaprevir every 8 hours for 12 weeks. Serum HCV RNA (upper panel) and the amino acid (aa) frequencies at aa156 in the HCV NS3 region by ultra-deep sequencing at the indicated times are shown. The horizontal dotted line indicates the detectable limit (1.2 log copy/mL).

multiple genomes using the Illumina Genome Analyzer. Briefly, cDNA was fragmented using sonication and the resultant fragment distribution was assessed using the Agilent BioAnalyzer 2100 platform. A library was prepared using the Multiplexing Sample Preparation Kit (Illumina, CA). Imaging analysis and base calling were performed using Illumina Pipeline software with default settings.[17-23] The N-terminal 543 nucleotides of NS3 protease were analyzed. This technique revealed an average coverage depth of over 1,000 sequence reads per basepair in the unique regions of the genome. Read mapping to a reference sequence was performed using Bowtie.[24] Because of the short 36 nucleotide read length, mapping hypervariable regions with multiple closely spaced variants against a reference sequence yields poor coverage. Therefore, common variants were identified by relaxing the mismatch settings as well as using *de novo* assembly using ABySS.[25] Multiple alternative reference sequences were included to improve coverage in variable regions. Codon counts were merged and analyzed using R v. 2.12.

Results

Emergence of a Telaprevir-Resistant Variant in a Hepatitis C Patient Treated with Telaprevir and Analysis of the A156F Mutation. A 55-year-old woman infected with genotype 1b HCV was treated with 750 mg of telaprevir every 8 hours for 12 weeks (Fig. 1). After 1 weeks of treatment, serum HCV RNA titer decreased below the detectable limit (1.2 log copy/mL). However, HCV RNA titer became positive by week 4. By week 12, HCV RNA titer had increased to 4.8 log copy/mL and telaprevir treatment was discontinued. Because direct sequence analysis showed an A156F mutation in the NS3 region in the serum samples at 12 weeks, we performed ultra-deep sequence analysis and confirmed the high frequency (92.5%) of A156F mutation. Four weeks after cessation of treatment (at 16 weeks), sequence analysis revealed that the major strain had reverted to wildtype (99%). To analyze the replication ability and the susceptibility of the A156F mutation to telaprevir, 100 μL serum samples containing 10^4 copies of HCV obtained at week 12 were injected into human hepatocyte chimeric mice. Two wildtype HCV-inoculated mice became positive for HCV RNA 2 weeks after inoculation and serum HCV RNA titer increased to high levels (7.6 and 7.8 log copy/mL, respectively) at 6 weeks after inoculation (Fig. 2). In contrast to wildtype HCV-infected mice, a mouse inoculated with serum containing the A156F mutant developed measurable viremia at 4 weeks postinoculation, although serum HCV RNA titer remained low at 6 weeks (5.2 log copy/mL). Eight weeks after inoculation ultra-deep sequence analysis showed a high frequency (99.9%) of A156F mutation. From this point the mouse was administrated 200 mg/kg of telaprevir perorally twice a day for 4 weeks. However, this treatment resulted in no reduction in serum HCV RNA level. During the observation period the A156F mutation remained at

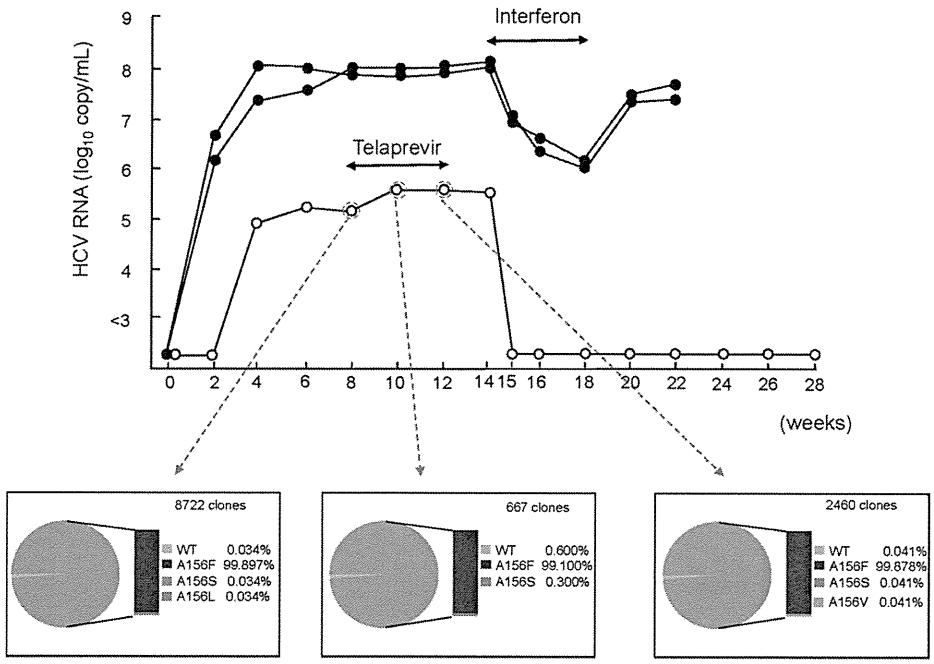

Fig. 2. Changes in serum virus titers in HCV-infected mice. Mice were injected with either wildtype (closed circles) or A156F-mutated HCV serum samples (obtained from an HCV-infected patient who received telaprevir monotherapy for 12 weeks; see Fig. 1) (open circles). Six weeks after injection the A156F mutant mouse was treated with 200 mg/kg of telaprevir orally twice a day for 4 weeks and injected intramuscularly with 1,500 IU/g/day of interferon-alpha for 4 weeks. Serum HCV RNA (upper panel) and amino acid (aa) frequencies at aa156 in the HCV NS3 region by ultra-deep sequencing at the indicated times are shown.

high frequency (>99%). To analyze the susceptibility of the A156F mutation to IFN, wildtype or A156F-mutated HCV-infected mice were treated with 1,500 IU/g/day of IFN-alpha for 4 weeks. Treatment resulted in only a two log reduction in HCV RNA level in wildtype HCV-infected mice. In contrast, serum HCV RNA titer decreased below the detectable limit 1 week after treatment in an A156F-infected mouse. Ten weeks after cessation of IFN-treatment (at week 28), HCV RNA in the mouse serum remained undetectable, suggesting that HCV RNA was eliminated. These results demonstrate that the A156F variant is associated with telaprevir-resistance, but the mutant has low replication ability and a high susceptibility to IFN.

Effect of Telaprevir on HCV-Infected Mice and Sequence Analysis of NS3 Region. Next we investigated the effect of telaprevir on wildtype HCV-infected mice. Two chimeric mice were inoculated intravenously with serum samples containing 10^5 copies of HCV obtained from an HCV-positive patient (Fig. 3). Six weeks after inoculation both mice were administered 200 mg/kg of telaprevir perorally twice a day for 4 weeks. Serum HCV RNA titer in both mice rapidly decreased; however, in one of the mice HCV RNA titer increased again 3 weeks after the start of treatment. Ultra-deep sequence analysis of the NS3 region showed that following the start of telaprevir administration the frequency of the V36A mutation increased from 18% at 2 weeks to 52% at 4 weeks, at which point it was accompanied by an increase in the HCV RNA titer. Two weeks after cessation of telaprevir treatment (at week 12), ultra-deep sequence analysis revealed that the frequency of the V36A mutant had decreased to 13% and the frequency of the wildtype HCV had increased to 84%, although the HCV RNA titer increased only slightly.

Intrahepatic Injection of HCV-KT9-Wild RNA and KT9-NS3-A156S RNA into Human Hepatocyte Chimeric Mice. We previously established an infectious genotype 1b HCV clone, HCV-KT9 (HCV-KT9-wild).[15] We created a telaprevir-resistant HCV clone by introducing an A156S amino acid substitution in the NS3 region of HCV-KT9 (KT9-NS3-A156S) (Fig. 4A). Using wildtype and telaprevir-resistant clones we investigated the replication ability *in vivo*. Mice were injected intrahepatically with 30 μg of *in vitro*-transcribed HCV-KT9-wild RNA or KT9-NS3-A156S RNA. Mice injected with HCV-KT9-wild developed measurable viremia at 2 weeks postinoculation and by 4 weeks postinoculation HCV RNA had reached 10^7 copy/mL (Fig. 4B). On the other hand, mice injected with KT9-NS3-A156S developed measurable viremia at 4 weeks postinoculation but maintained only low levels of viremia. These results suggest that the telaprevir-resistant HCV clone has a lowered replication ability compared to the wildtype HCV clone *in vivo*.

Treatment with Telaprevir and Analysis of Mutagenesis in Mice. Two mice infected with HCV-KT9-wild and one mouse infected with KT9-NS3-A156S were treated with 200 mg/kg of telaprevir twice a day for 2 weeks (Fig. 5A), resulting in 1.4 and 2.7 log

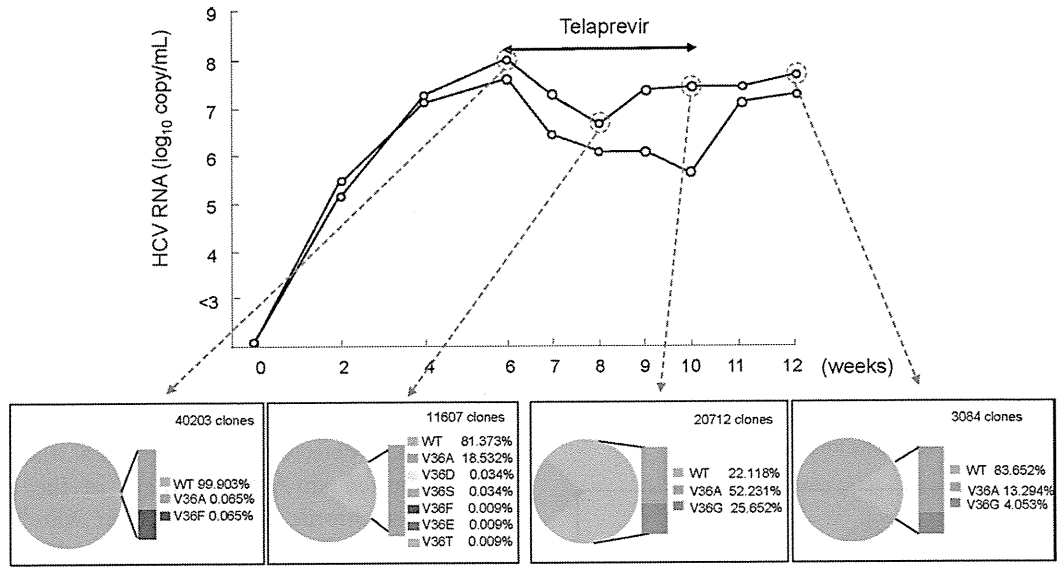

Fig. 3. Treatment with telaprevir in wildtype HCV-infected mice. Two mice were injected intravenously with 50 μL of HCV-positive human serum samples. Six weeks after HCV injection mice were treated with 200 mg/kg of telaprevir orally twice a day for 4 weeks. Serum HCV RNA (upper panel) and amino acid (aa) frequencies at aa36 in the HCV NS3 region by ultra-deep sequencing at the indicated times are shown.

reductions in HCV RNA level in the two wildtype HCV-infected mice. In contrast, only a 0.6 log reduction was observed in the KT9-NS3-A156S-infected mouse. These results demonstrate that our human hepatocyte chimeric mouse model infected with *in vitro*-transcribed HCV RNA provides an effective system for analysis of the susceptibility of HCV mutants to antiviral drugs. Interestingly, ultra-deep sequence analysis showed a rapid emergence of a V36A variant in the NS3 region in mouse serum 2 weeks after treatment (Fig. 5B). Four weeks after cessation of treatment (at week 6) the frequency of the V36A variant had decreased. Mice were then treated with 300 mg/kg of telaprevir twice a day for 4 weeks, which resulted in an elevated frequency of V36A variants at 1 (at week 7, 5.4%) and 4 weeks (at 10 week, 41.8%) after treatment and no reduction in serum HCV RNA level. These results suggest that telaprevir-resistant mutations emerged *de novo* from the wildtype strain of HCV, presumably through error-prone replication and potent selection for telaprevir escape mutants. During the telaprevir treatment period no increases of HCV RNA titers in these mice were observed, probably due to the low frequency of the resistant strain.

Discussion

Telaprevir is a peptidomimetic inhibitor of the NS3-4A serine protease that is currently undergoing clinical evaluation. Despite its effectiveness against HCV, some patients have shown a rapid viral breakthrough during the first 14 days of treatment.[26] Population sequencing of the viral NS3 region identified a number of mutations near the NS3 protease catalytic

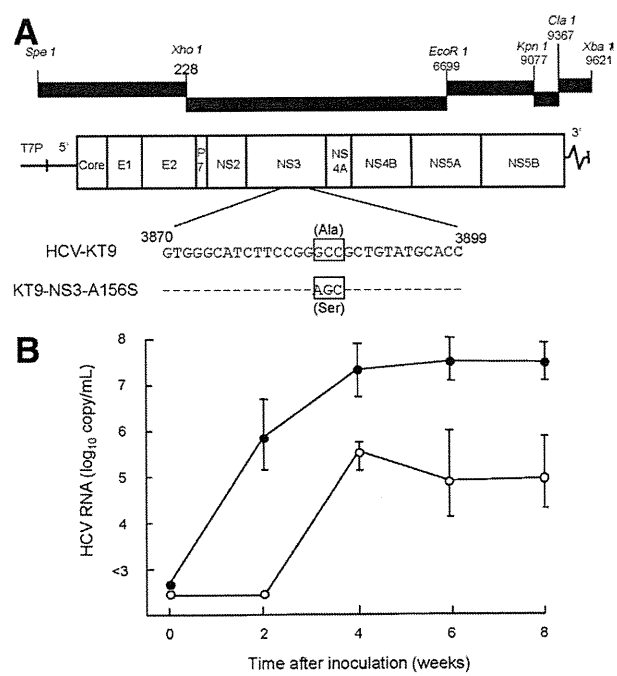

Fig. 4. Intrahepatic injection of *in vitro* transcribed HCV-KT9 RNA and KT9-NS3-A156S RNA into human hepatocyte chimeric mice. (A) The schematic of infectious genotype 1b HCV clones, HCV-KT9 and KT9-NS3-A156S. Boxes indicate codons at amino acid 156 in HCV NS3 region. Ala, alanine; Ser, serine. (B) Changes in serum levels of HCV RNA in mice intrahepatically injected with either HCV-KT9 RNA (closed circles) or KT9-NS3-A156S RNA (open circles). Data are represented as the mean ± SD of three mice.

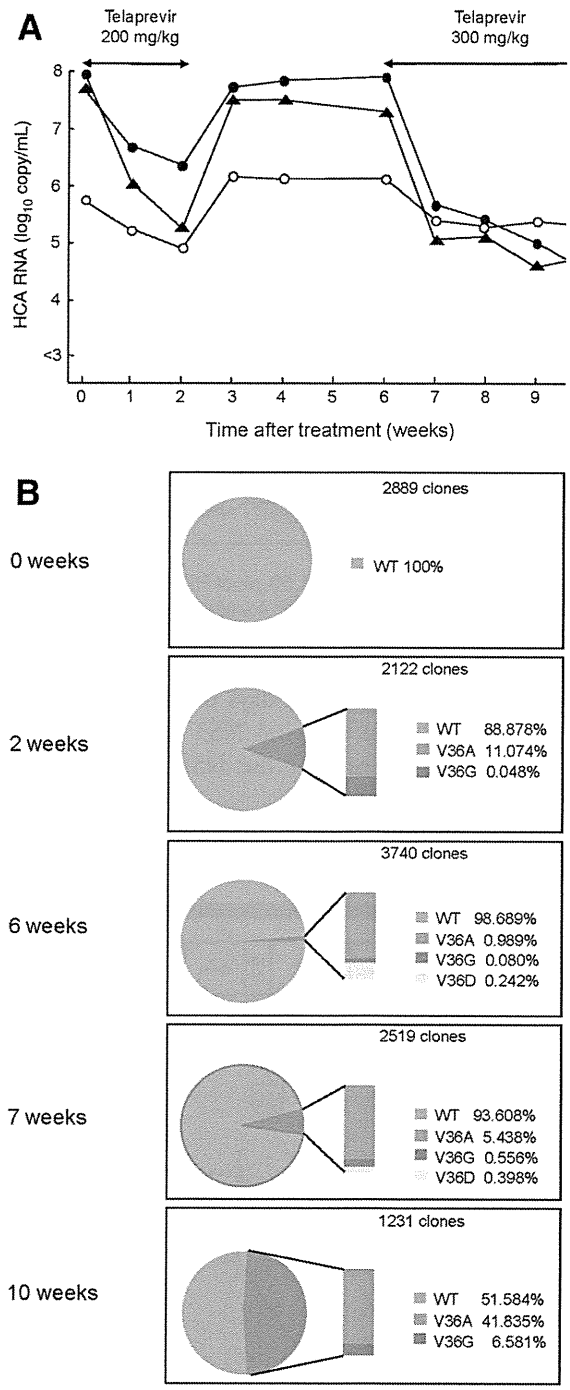

Fig. 5. The effect of telaprevir on mice infected with *in vitro*-transcribed HCV. Mice were injected with *in vitro*-transcribed HCV-KT9 RNA (closed circles and closed triangles) or KT9-NS3-A156S RNA (open circles). Six weeks after HCV RNA injection, mice were treated perorally with 200 mg/kg of telaprevir twice a day for 2 weeks. Four weeks after cessation of treatment mice were treated with 300 mg/kg of telaprevir twice a day for 4 weeks. (A) Mice serum HCV RNA titers at the indicated times are shown. Serum samples obtained from one of two HCV-KT9-infected mice (closed triangles) were used for ultra-deep sequencing. (B) Amino acid (aa) frequencies at aa36 in the HCV NS3 region based on ultra-deep sequencing are shown.

domain.[26] In particular, variants at NS3 residues 36, 54, 155, and 156 were shown to confer reduced sensitivity to telaprevir.[27]

In this study we analyzed the association between the antiviral efficacy of telaprevir and sequence variants within the NS3 region using chimeric mice infected with serum samples obtained from an HCV genotype 1b-infected patient. One of two HCV-infected mice had a viral breakthrough during the dosing period (Fig. 3). Ultra-deep sequence analysis of the NS3 region showed an increase of the V36A mutant, which has been reported to confer telaprevir resistance.[26] Consequently, our results show evidence of emergence of a telaprevir-resistant variant previously detected in human clinical trials.

We detected an A156F mutant in the HCV NS3 region in a chronic hepatitis patient who had experienced viral breakthrough during telaprevir monotherapy (Fig. 1). Likewise, HCV RNA titer in mice infected with the A156F variant showed no reduction following 2 weeks of telaprevir treatment (Fig. 2). However, 2 weeks of treatment with IFN-alpha rapidly suppressed serum HCV RNA titer below the detectable limit. These results demonstrate that A156F is telaprevir-resistant but has a high susceptibility to IFN.

Interestingly, ultra-deep sequencing revealed that the wildtype strain was present at low frequency (0.3%) in the serum inoculum (Fig. 2). However, the frequency of the wildtype failed to increase over time (Fig. 3), suggesting that the very small number of wildtype viral RNA (about 30 copies) may be incomplete or defective, as a large proportion of viral genomes are thought to be defective due to the virus's high replication and mutation rates.[9] Further analysis is necessary in order to interpret the significance of the presence of very low frequency variants detected by ultra-deep sequencing.

The short read lengths used in next generation sequencing also complicates the detection of rare variants, especially when variants are clustered within a region smaller than an individual read length (e.g., 36 basepairs). Relaxing the matching criteria allows mapping of more diverse reads but increases the error rate, whereas default settings may be geared toward more genetically homogenous haploid or diploid genomes. In this study we used *de novo* assembly to identify more diverse variants that failed to map to the reference sequence. Examining the variation in codon frequencies among samples, we created alternative reference sequences containing a sufficient range of variants to provide more uniform coverage of variable regions.

Using our previously established infectious HCV-KT9 genotype 1b HCV clone, we investigated the antiviral efficacy of telaprevir and the effect of

resistance mutations on viral replication. HCV RNA titer in mice infected with the telaprevir-resistant strain KT9-NS3-A156S was lower than in mice infected with the wildtype strain HCV-KT9-wild (Fig. 4B). HCV NS proteins include proteases for sequential processing of the polyprotein and are thought to be important in viral replication.[28] Our results suggest that differences in viral fitness underlie the differences in viral replication capacity. We analyzed the antiviral efficacy of telaprevir and the sequence of the NS3 region using HCV-infected mice treated with telaprevir. Although telaprevir treatment suppressed serum HCV RNA titer in mice infected with HCV-KT9, the decline of HCV RNA titer was only 0.6 log copy/mL in a mouse infected with KT9-NS3-A156S under the same treatment (Fig. 5A). These results suggest that our genetically engineered HCV-infected mouse model is useful for analyzing HCV escape mutants associated with antiviral drugs. Interestingly, treatment with telaprevir resulted in selection for V36A variants in the NS3 region in an HCV-KT9-infected mouse (Fig. 5B). There are a few controversial reports proposing that resistant variants may already be present at low frequency (<1%) within the quasispecies population in treatment-naïve patients,[29] consistent with their rapid emergence only days after treatment initiation.[26,30] This might well occur, due to the large number of mutated HCV clones. However, our results provide evidence in support of *de novo* emergence of telaprevir resistance induced by viral mutation followed by selection. HCV has both a high replication rate (10^{12} particles per day) and a high mutation rate (10^{-3} to 10^{-4}),[9,10] suggesting that the viral quasispecies population is likely to represent a large and genetically diverse substrate for immune selection.

In summary, we established an infection model of a genotype 1b HCV clone using the human hepatocyte chimeric mouse model. Using this model we demonstrate rapid emergence of *de novo* telaprevir-resistant HCV quasispecies from wildtype HCV.

Acknowledgment: The authors thank Rie Akiyama, Kazuyo Hattori, Yoshie Yoshida, Kiyomi Toyota, and Yoko Matsumoto for expert technical assistance.

References

1. Kiyosawa K, Sodeyama T, Tanaka E, Gibo Y, Yoshizawa K, Nakano Y, et al. Interrelationship of blood transfusion, non-A, non-B hepatitis and hepatocellular carcinoma: analysis by detection of antibody to hepatitis C virus. HEPATOLOGY 1990;12:671-675.
2. Niederau C, Lange S, Heintges T, Erhardt A, Buschkamp M, Hurter D, et al. Prognosis of chronic hepatitis C: results of a large, prospective cohort study. HEPATOLOGY 1998;28:1687-1695.
3. Manns MP, McHutchison JG, Gordon SC, Rustgi VK, Shiffman M, Reindollar R, et al. Peginterferon alfa-2b plus ribavirin compared with interferon alfa-2b plus ribavirin for initial treatment of chronic hepatitis C: a randomised trial. Lancet 2001;358:958-965.
4. Fried MW, Shiffman ML, Reddy KR, Smith C, Marinos G, Goncales FL Jr, et al. Peginterferon alfa-2a plus ribavirin for chronic hepatitis C virus infection. N Engl J Med 2002;347:975-982.
5. Hoofnagle JH, Ghany MG, Kleiner DE, Doo E, Heller T, Promrat K, et al. Maintenance therapy with ribavirin in patients with chronic hepatitis C who fail to respond to combination therapy with interferon alfa and ribavirin. HEPATOLOGY 2003;38:66-74.
6. Perni RB, Almquist SJ, Byrn RA, Chandorkar G, Chaturvedi PR, Courtney LF, et al. Preclinical profile of VX-950, a potent, selective, and orally bioavailable inhibitor of hepatitis C virus NS3–4A serine protease. Antimicrob Agents Chemother 2006;50: 899-909.
7. Lin C, Gates CA, Rao BG, Brennan DL, Fulghum JR, Luong YP, et al. In vitro studies of cross-resistance mutations against two hepatitis C virus serine protease inhibitors, VX-950 and BILN 2061. J Biol Chem 2005;280:36784-36791.
8. Mo H, Lu L, Pilot-Matias T, Pithawalla R, Mondal R, Masse S, et al. Mutations conferring resistance to a hepatitis C virus (HCV) RNA-dependent RNA polymerase inhibitor alone or in combination with an HCV serine protease inhibitor in vitro. Antimicrob Agents Chemother 2005;49:4305-4314.
9. Bartenschlager R, Lohmann V. Replication of hepatitis C virus. J Gen Virol 2000;81:1631-1648.
10. Rong L, Dahari H, Ribeiro RM, Perelson AS. Rapid emergence of protease inhibitor resistance in hepatitis C virus. Sci Transl Med 2010;2: 30ra32.
11. Mercer DF, Schiller DE, Elliott JF, Douglas DN, Hao C, Rinfret A, et al. Hepatitis C virus replication in mice with chimeric human livers. Nat Med 2001;7:927-933.
12. Kneteman NM, Weiner AJ, O'Connell J, Collett M, Gao T, Aukerman L, et al. Anti-HCV therapies in chimeric scid-Alb/uPA mice parallel outcomes in human clinical application. HEPATOLOGY 2006;43: 1346-1353.
13. Kamiya N, Iwao E, Hiraga N, Tsuge M, Imamura M, Takahashi S, et al. Practical evaluation of a mouse with chimeric human liver model for hepatitis C virus infection using an NS3–4A protease inhibitor. J Gen Virol 2010;91:1668-1677.
14. Hiraga N, Imamura M, Tsuge M, Noguchi C, Takahashi S, Iwao E, et al. Infection of human hepatocyte chimeric mouse with genetically engineered hepatitis C virus and its susceptibility to interferon. FEBS Lett 2007;581:1983-1987.
15. Kimura T, Imamura M, Hiraga N, Hatakeyama T, Miki D, Noguchi C, et al. Establishment of an infectious genotype 1b hepatitis C virus clone in human hepatocyte chimeric mice. J Gen Virol 2008;89: 2108-2113.
16. Tateno C, Yoshizane Y, Saito N, Kataoka M, Utoh R, Yamasaki C, et al. Near completely humanized liver in mice shows human-type metabolic responses to drugs. Am J Pathol 2004;165:901-912.
17. Cronn R, Liston A, Parks M, Gernandt DS, Shen R, Mockler T. Multiplex sequencing of plant chloroplast genomes using Solexa sequencing-by-synthesis technology. Nucleic Acids Res 2008;36:e122.
18. Mitsuya Y, Varghese V, Wang C, Liu TF, Holmes SP, Jayakumar P, et al. Minority human immunodeficiency virus type 1 variants in antiretroviral-naive persons with reverse transcriptase codon 215 revertant mutations. J Virol 2008;82:10747-10755.
19. Margeridon-Thermet S, Shulman NS, Ahmed A, Shahriar R, Liu T, Wang C, et al. Ultra-deep pyrosequencing of hepatitis B virus quasispecies from nucleoside and nucleotide reverse-transcriptase inhibitor (NRTI)-treated patients and NRTI-naive patients. J Infect Dis 2009; 199:1275-1285.
20. Szpara ML, Parsons L, Enquist LW. Sequence variability in clinical and laboratory isolates of herpes simplex virus 1 reveals new mutations. J Virol 2010;84:5303-5313.

21. Wright CF, Morelli MJ, Thebaud G, Knowles NJ, Herzyk P, Paton DJ, et al. Beyond the consensus: dissecting within-host viral population diversity of foot-and-mouth disease virus by using next-generation genome sequencing. J Virol 2011;85:2266-2275.
22. Verbinnen T, Van Marck H, Vandenbroucke I, Vijgen L, Claes M, Lin TI, et al. Tracking the evolution of multiple in vitro hepatitis C virus replicon variants under protease inhibitor selection pressure by 454 deep sequencing. J Virol 2010;84:11124-11133.
23. Wang GP, Sherrill-Mix SA, Chang KM, Quince C, Bushman FD. Hepatitis C virus transmission bottlenecks analyzed by deep sequencing. J Virol 2010;84:6218-6228.
24. Langmead B, Trapnell C, Pop M, Salzberg SL. Ultrafast and memory-efficient alignment of short DNA sequences to the human genome. Genome Biol 2009;10:R25.
25. Simpson JT, Wong K, Jackman SD, Schein JE, Jones SJ, Birol I. ABySS: a parallel assembler for short read sequence data. Genome Res 2009;19:1117-1123.
26. Sarrazin C, Kieffer TL, Bartels D, Hanzelka B, Muh U, Welker M, et al. Dynamic hepatitis C virus genotypic and phenotypic changes in patients treated with the protease inhibitor telaprevir. Gastroenterology 2007;132:1767-1777.
27. Kuntzen T, Timm J, Berical A, Lennon N, Berlin AM, Young SK, et al. Naturally occurring dominant resistance mutations to hepatitis C virus protease and polymerase inhibitors in treatment-naive patients. HEPATOLOGY 2008;48:1769-1778.
28. Hijikata M, Mizushima H, Tanji Y, Komoda Y, Hirowatari Y, Akagi T, et al. Proteolytic processing and membrane association of putative nonstructural proteins of hepatitis C virus. Proc Natl Acad Sci U S A 1993;90:10773-10777.
29. Lu L, Mo H, Pilot-Matias TJ, Molla A. Evolution of resistant M414T mutants among hepatitis C virus replicon cells treated with polymerase inhibitor A-782759. Antimicrob Agents Chemother 2007;51:1889-1896.
30. Kieffer TL, Sarrazin C, Miller JS, Welker MW, Forestier N, Reesink HW, et al. Telaprevir and pegylated interferon-alpha-2a inhibit wild-type and resistant genotype 1 hepatitis C virus replication in patients. HEPATOLOGY 2007;46:631-639.

ELSEVIER

Cancer Genetics 205 (2012) 18–24

Cancer Genetics

Microarray CGH analyses of chromosomal 20q deletions in patients with hematopoietic malignancies

Michiko Okada [a,*], Yumiko Suto [b], Momoki Hirai [c], Masayuki Shiseki [d], Akemi Usami [a], Kaori Okajima [a], Masanao Teramura [d], Naoki Mori [d], Toshiko Motoji [d]

[a] *Chromosome Laboratory, Shiseikai Dai-Ni Hospital, Tokyo, Japan;* [b] *Central Blood Institute, Japanese Red Cross Society, Tokyo, Japan;* [c] *International Research and Educational Institute for Integrated Medical Science, Tokyo Women's Medical University, Tokyo, Japan;* [d] *Division of Hematology, School of Medicine, Tokyo Women's Medical University, Tokyo, Japan*

The chromosomal abnormality del(20q) is mostly found in various myeloid disorders, including myelodysplastic syndromes, myeloproliferative neoplasms, and acute myeloid leukemia. Here, microarray comparative genomic hybridization (aCGH) analyses of 14 patients cytogenetically confirmed to carry the del(20q) aberration in their bone marrow demonstrated that all deletions were interstitial and both the proximal and distal breakpoints varied among individuals. The centromeric breakpoints were located in the 20q11.21-12 region, and the telomeric breakpoints, in the 20q13.13-13.33 region. The extent of the deletion ranged from 11.2 to 27.3 Mb, and the commonly deleted region (CDR) was estimated to be 7.2 Mb in size. Two commonly retained regions were present, the proximal region adjacent to the centromere (20q11.1-11.21) and a subtelomeric one (20q13.33). The CDR of our study was more distal than reported previously. Furthermore, in three patients fluorescence in situ hybridization (FISH) demonstrated that del(20q) cells were detected at a higher frequency in the karyotype analyses than by interphase FISH and aCGH analyses. As the size and breakpoints of del(20q) have been reported to vary among patients, the presence of one or more tumor suppressor genes in the CDR has been suggested. Our study will contribute to the identification of candidate tumor suppressor genes on 20q.

Keywords Hematopoietic malignancies, del(20q) chromosome, microarray comparative genomic hybridization, commonly deleted region, interphase fluorescence in situ hybridization

The chromosomal abnormality del(20q) is found in various myeloid disorders, including myelodysplastic syndromes (MDSs), myeloproliferative neoplasms (MPNs), and acute myeloid leukemia (AML). MDS patients with a del(20q) have a relatively good prognosis (1). The deletion has been reported to be rare in patients with lymphoid malignancies (2), although it can arise in multipotent precursors of myeloid cells and B cells (3) and in pluripotent stem cells (4). However, during the last 20 years, we observed lymphoid malignancies in 8 of 73 patients who had del(20q) in their bone marrow cells. Therefore, we included two lymphoid patients in this study.

Received October 9, 2010; received in revised form December 2, 2011; accepted December 2, 2011.

* Corresponding author.
E-mail address: okadam@dh.twmu.ac.jp

Delineation of the bands deleted on 20q is difficult using conventional cytogenetic techniques because of the small size and indistinct banding, especially in bone marrow samples. The deletions were suggested to be interstitial and grouped into two categories, large deletions involving the loss of both G(+) bands from 20q and small deletions involving the loss of one G(+) band (20q12) (5). Molecular studies of del(20q) have defined a commonly deleted region (CDR) of 1.7–6.62 Mb using bacterial artificial chromosome (BAC)/P1-derived artificial chromosome (PAC) fluorescence in situ hybridization (FISH) or microsatellite polymerase chain reaction (PCR) (6,7). Recently, Huh et al. reported two CDRs, of 2.5 Mb and 1.8 Mb (8).

We preliminarily estimated the CDR of del(20q) to be 8.2 Mb in length from a study of eight patients at the Third Asian Chromosome Colloquium (ACC3) (9) using microarray

2210-7762/$ - see front matter © 2012 Elsevier Inc. All rights reserved.
doi:10.1016/j.cancergen.2011.12.002

comparative genome hybridization (aCGH) analyses. In the present report, we have added four more patients and reduced the estimated length of the CDR to 7.2 Mb. The purpose of this study was to accurately characterize del(20q) chromosomes from 12 patients with hematopoietic malignancies. Using 60-mer oligonucleotide arrays, we characterized their proximal and distal breakpoints in chromosome 20 to be between 30,100,973–39,933,662 bp, and 47,180,979–58,444,848 bp, (build 36.1, hg18) respectively.

Materials and methods

The experimental protocol involved the following steps: (A) Chromosomes were analyzed in bone marrow aspirates from 14 patients (Table 1). A portion of the aspirates and the rest of the fixed cells after the chromosome analysis were stored at −20°C. (B) We conducted aCGH analyses on the fixed cells or the bone marrow aspirates after storage for 0.5–8 years (Table 2). (C) The preserved cells of three patients, who showed differences in clone size by karyotype and array analyses, were used for FISH and additional karyotype analyses about 2 years after the array experiments (Table 3).

Patients

We selected 14 patients with a deletion of the long arm of chromosome 20, detected by Q-banding, for aCGH analyses. Six of the patients had MDS, one had MPN, five had AML, and two had lymphoid malignancies, Waldenström macroglobulinemia (WM) and non-Hodgkin lymphoma (NHL) in a leukemic phase (Table 1). The patients were diagnosed using the World Health Organization (WHO) classifications for myeloid neoplasms and acute leukemia (10), and hematopoietic and lymphoid tissues (11).

Chromosome analyses

Chromosome examinations were performed with a Q-banding technique using bone marrow cells cultured overnight without any mitogens, except in patient 12. A 7-day culture in the presence of phorbol 12-myristate 13-acetate (TPA) was also used for karyotype analyses of patient 12 to stimulate B-cell–lineage growth (Table 1). Karyotypes were described according to the International System for Human Cytogenetic Nomenclature 2009 (12).

Microarray CGH analyses

DNA was extracted from uncultured bone marrow aspirates from six patients. In the other eight patients, bone marrow cells fixed in Carnoy solution were used after an unstimulated overnight culture. All of these specimens had been preserved at −20°C for 0.5–8 years. The fixed cells were washed three times with 99% ethanol before use. DNA was isolated with a genomic DNA preparation kit (Mammalian Genome Mini Prep, Sigma-Aldrich, St. Louis, MO). Pooled human DNA (Promega, Fitchburg, WI) was used as a reference. The microarrays used in this study were 60-mer in situ synthesized oligonucleotide arrays produced by Agilent Technologies (Santa Clara, CA) based on the Human March 2006 Assembly (National Center for Biotechnology Information [NCBI], build 36.1, hg18). We used a genomewide catalogue CGH array consisting of approximately 244,000 probes with a mean interprobe interval of 8.9 b. All hybridizations were

Table 1 Clinical and cytogenetic characteristics of patients

Patient	Diagnosis	Sex/Age, y	Karyotype
1	MDS(RA)	M/73	46,XY,del(20)(q13.1 or q13.1q13.3)[26]/46,XY[3]
2	MDS(RA)	F/51	46,XX,del(20)(q11.2)[22]
3	MDS(RCMD)	M/69	46,XY,del(20)(q11.2)[30]
4	MDS(RCMD)	F/84	46,XX,del(20)(q11.1q13.1∼13.2) or del(20)(q13.1q13.3)[26]/46,XX[2]
5	MDS(RCMD)	M/76	46,XY,del(20)(q11q13.3)[11]/46,XY[16]
6	MPN(PV)	M/85	46,XY,del(20)(q11.?2q13.?1)[33]
7	MDS(RCMD)→AML	M/72	46,XY,del(20)(q11.2q13.3)[25]
8	MDS(RCMD)→AML	M/69	47,XY,+8,del(20)(q12 or q11q13.1)[30]
9	MPN(ET)→AML	M/65	46,XY,+1,der(1;7)(q10;p10),del(20)(q11.2 or q11.1q13.3)[30]
10	AML	F/74	47,XX,+8,del(20)(q11.2q13.1∼13.2)[32]
11	AML	M/76	46,XY,inv(9)(p12q13),der(16)t(1;16)(q12∼21;q11∼12)[1]/46,idem, del(20)(q11)[29]
12	WM	M/75	46,XY,inv(9)(p12q13),del(20)(q11.2)[25]/46,XY,inv(9)(p12q13)[3] (overnight culture without any stimulation) 46,XY,inv(9)(p12q13),del(20)(q11.2)[15]/ 46,XY,del(7)(q21q36),inv(9)(p12q13)[1]/46,XY,inv(9)(p12q13)[8] (7-day culture with TPA stimulation)
13	NHL in a leukemic phase	F/83	46,XX,del(20)(q11.2q13.3)[14]/46,XX[15]
14	MDS(RCMD)	M/63	46,XY,del(20)(q12q13.3)[9]/46,XY[17]
15[a]	AML with inv(16) (p13.1q22) in CR	M/36	46,XY[29]

Abbreviations: RA, refractory anemia; RCMD, refractory cytopenia with multilineage dysplasia; PV, polycythemia vera; ET, essential thrombocythemia.

[a] This is a control patient in the FISH experiment with no history of carrying a del(20q), and not included in aCGH studies.

Table 2 Results of aCGH analyses

Patient	Start (NT)	End (NT)	Deletion size (Mb)	Deleted bands detected by array analysis
1	37,488,367	50,316,897	12.83	20q12-13.2
2	30,411,323	49,098,594	18.69	20q11.21-13.13
3	30,319,299	51,455,290	21.14	20q11.21-13.2
4	36,957,293	54,407,570	17.45	20q11.23-13.31
5	31,134,883	58,444,848	27.31	20q11.21-13.33
6	32,233,259	47,180,979	14.95	20q11.22-13.13
7	31,049,105	49,076,424	18.03	20q11.21-13.13
8	34,408,519	48,145,526	13.74	20q11.23-13.13
9	34,049,128	50,034,067	15.98	20q11.23-13.2
10	39,933,662	51,171,130	11.24	20q12-13.2
11	34,351,399	57,476,399	23.13	20q11.23-13.32
12	30,100,973	56,986,098	26.89	20q11.21-13.32
13	Deletion was not detected in these two patients			
14				

Abbreviation: NT, nucleotide number.

performed according to the manufacturer's recommended protocols.

The restriction enzymes *AluI* and *RsaI* were used to digest 500 ng of genomic DNA, which we then fluorescently labeled using an Agilent Genomic Labeling Kit. The test samples were labeled with cyanine 5-deoxyuridine triphosphate, and the reference samples were labeled with cyanine 3-deoxyuridine triphosphate. Labeled DNA was denatured and pre-annealed with human Cot-1 DNA (Invitrogen, Carlsbad, CA) and Agilent blocking reagent prior to hybridization for 40 hours at 20 rpm in a 65°C hybridization oven. Standard washing procedures were followed. Array slides were scanned (GenePix 4000B; Axon Instruments, Foster City, CA) at a resolution of 5 mm, and image analysis was performed using the default CGH settings of Feature Extraction Software 9.1.3.1 (Agilent Technologies). Agilent Genome Workbench 5.0 was used to visualize, detect, and analyze genomic gain/loss patterns in the aCGH profiles using the ADM-2 algorithm and the optimum analytical conditions (threshold 6.0, default value).

FISH analyses

FISH experiments were performed on 3 patients (patients 12, 13, and 14) and a control (patient 15). Slides were prepared from the stored cells of overnight cultures described in the chromosome analyses. Karyotypes were additionally analyzed on those slides in each patient. A dual-color FISH probe was used to estimate the clone size of del(20q) cells. The probe was a mixture of the approximately 450-kb Texas Red–labeled *PTPRT* gene probe (composed of 3 BAC clones, GSP1579H07, GSP1187C03, and GSP1586H05) and 680-kb fluorescein isothiocyanate (FITC)–labeled DNA BAC clones (GSP1226G02, GSP1558G11, GSP1546F12, and GSP1152H07) designed by Genomic Signal Processing Laboratory (Kawasaki City, Japan). The *PTPRT* gene is located at 20q12~q13, the most proximal region within our CDR. The FITC-labeled probe is at 20q11.22, 5 Mb from the *PTPRT* gene. Del(20q) cells with large deletions (patients 12 and 13) were expected to have one green and one red signal.

Table 3 Results of FISH analysis

	Del(20q) chromosome[a]			FISH pattern of dual-color 20q probe			
				No. of cells with the pattern (%)			
Patient	Banding	No. of cells with del(20q) (%)	Total observed cells	G2R1[b]	G1R1[c]	G2R2[d]	Total
12	del(20)(q11.2)	24 (80.0)	30	I 7(1.9)	83(22.4)	280(75.7)	370
				M 0(0.0)	4(66.7)	2(33.3)	6
13	del(20)(q11.2q13.3)	3 (30.0)	10	I 10(2.2)	59(12.9)	388(84.9)	457
				M	ND		
14	del(20)(q12q13.3)	4 (23.5)	17	I 24(11.7)	5(2.4)	176(85.9)	205
				M	ND		
15 (control)	Normal karyotype	0 (0.0)	29	I 4(1.9)	1(0.5)	200(97.6)	205
				M	ND		

Abbreviations: I, interphase; M, metaphase; ND, no determination.

[a] Chromosomes were analyzed additionally on slides prepared for FISH experiments.

[b] G2R1 is a FISH pattern with 2 green and 1 red signal. Del(20q) cells of patient 14 demonstrate this pattern in the interphase nuclei.

[c] G1R1 is a FISH pattern with 1 green and 1 red signal. Del(20q) cells of patient 12 and patient 13 demonstrate this pattern.

[d] G2R2 is a FISH pattern with 2 green and 2 red signals, the pattern of cells having 2 normal chromosome 20.